Dedication

A ma femme, Annie, dont la patience et le courage
sont l'encre même de ces pages

STATE PLANE ANALYSIS OF INDUCTION HOB GENERATORS

by

Sean Carthy B Sc

Thesis presented for the degree of
Doctor of Philosophy

supervised by

Dr G Rilly, D T B GmbH, Villingen, Germany
Dr J Ringwood, School of Electronic Engineering, D C U

Dublin City University, March, 1994

I hereby certify that this material, which I now submit for assessment on the programme of study leading to the award of Doctor of Philosophy is entirely my own work and has not been taken from the work of others save and to the extent that such work has been cited and acknowledged within the text of my work

Signed Seán Carthy Date 24/3/94

Acknowledgements

I wish to thank all those who have contributed over the last five and a half years with encouragement, advice, and help on practicalities

I particularly want to thank Dr Gerard Rilly without whom this thesis would never have seen the light of day His guidance and encouragement were instrumental in seeing the research work through to a valid conclusion

I am grateful to Dr John Ringwood, my supervisor, and to Gerard Morizot for his helpful comments and proof reading of this thesis

I also want to thank Professor Jean-Marie Peter for having consented to being my external examiner

Thanks are also due to my employer, Deutsche Thomson Brandt GmbH, for use of the equipment

Contents

Contents 1

Abstract 3

Preface 4

1 INTRODUCTION 6
- 1 1 Induction heating 6
- 1 2 Induction cooking 6
- 1 3 Series Resonant Converter (SRC) 8
  - 1 3 1 Output plane 10
  - 1 3 2 State plane 10
- 1 4 SRC in induction 12
- 1 5 Load measurement 13

2 THE INDUCTION HOB 15
- 2 1 Introduction 15
- 2 2 The power part 17
  - 2 2 1 Mains filtering 17
  - 2 2 2 Supply voltage 17
  - 2 2 3 Generator structure 18
  - 2 2 4 Dimensions 21
- 2 3 Choice of active power switches 21
  - 2 3 1 BJT 22
  - 2 3 2 MOSFET 23
  - 2 3 3 IGBT 24
  - 2 3 4 Conclusions 25
- 2 4 Transistor control mechanism 26
- 2 5 Control electronics 29
- 2 6 Inductor 30
- 2 7 User interface 32
- 2 8 Housing 32

3 STATE PLANE STEADY-STATE ANALYSIS OF INDUCTION SRC 35
- 3 1 Introduction 35
- 3 2 General solution for free oscillations 35
  - 3 2 1 Initial conditions 37

3 3 Forced oscillations 38
3 3 1 Limit cycle 40
3 4 Construction 41
3 5 CCM 1 construction 41
3 5 1 CCM 1 - T control 41
3 5 2 CCM 1 - T_C control 42
3 6 CCM 2 construction 43
3 6 1 CCM 2 - T control 45
3 6 2 CCM 2 - T_D control 45

4 GENERAL OBSERVATIONS ON SRC THROUGH STATE PLANE 47
4 1 Introduction 47
4 2 Time domain representation 47
4 3 Comparison of T and T_C control 50
4 4 Max diode and transistor conduction time 51
4 5 Capacitive switching-aid network 53
4 5 1 Steady-state with fixed axes 53
4 5 2 Steady-state with capacitive switching-aid network 54

5 LOAD MEASUREMENT IN INDUCTION HEATING APPLICATIONS 58
5 1 Introduction 58
5 2 Analysis 58
5 3 Measurement, filtering and verification 59
5 4 Results 63
5 5 Conclusions 66

General Conclusion 68

References 70

APPENDIX A STEADY-STATE ANALYSIS BASED ON V_C A 1
A 1 Limit cycle A 1
A 2 CCM 1 - T control A 2
A 3 CCM 1 - T_C control A 3

APPENDIX B ANALYTIC APPROACH TO STEADY-STATE OPERATION WITH T CONTROL B 1

Abstract

STATE PLANE ANALYSIS OF INDUCTION HOB GENERATORS

by

Sean Carthy B Sc

Induction cooking hobs have greatly gained in popularity in Europe during the 1980's This fact has focused attention on the particular problems encountered in their design To this day, the design approaches remain largely empirical This thesis presents an analysis technique specially adapted to the induction hob generator

The series resonant converter is seen to be widely used in the induction cooking application As a first step, a technique for determining steady-state operation of the converter is presented This is done for all the operation modes and control schemes encountered The technique in question is based on the well known state plane but has been adapted for use in induction This technique is then extended to make use of the properties of the state plane in order to demonstrate the behaviour of the converter under various load and control conditions At this point, the didactic qualities of the state plane representation are exploited to their full in order to demonstrate the intricate relationships between the operation of the series resonant converter and its load impedance

All of the work described in the previous paragraph is based on the assumption of knowing the load impedance of the converter This reveals itself to be a major assumption, given the variety of loads that can be encountered by an induction hob and the difficulties involved in measuring or modelling such a load In order to allow the verification of this technique with respect to real cases, a load measurement technique is presented This technique overcomes the pitfalls of existing techniques by carrying out analyses on wave forms measured in-situ while the converter is working This contrasts with the existing techniques which measure the isolated load at low signal levels

Preface

The work described in this thesis is a final contribution to a project which began in 1983 with the aim of developing an induction hob generator This generator had to meet the demands of the professional market and then allow an adaptation to the consumer market This work was carried out at Thomson Consumer Electronics advanced laboratories in Villingen, Germany with the co-operation of Bonnet S A in Villefranche-sur-Saone, France for the professional unit and Cepem S A in Orleans, France for the consumer unit

A transistorised professional unit was commercialised in 1988 and the consumer unit followed in 1990 both being based on the same principle The relationships governing the operation of these generators are complex A variety of simulation tools already exist in industry, but due to the difficulty in determining load impedance for a given utensil, the work had to be carried out in an empirical manner Although this approach has been successful, it has not given entire satisfaction

From 1988 research work was started in parallel with the continuing development work in order to find a simple technique which would allow the prediction of the behaviour of the generator circuit The research carried out on the question is the subject of this thesis

After a short preamble on the nature of the induction cooking problem pin-pointing two aspects, the generator and the load, chapter 1 shows that the state of the art in analysis of induction generators is poor The existing analysis techniques are either too complex and impractical or inapplicable and none gives any insight into the operation of the circuit A description of the possibilities of the existing load measuring or modelling techniques is not very positive either

The technological aspects of the project are given in chapter 2, with a description of the two induction units mentioned above It includes an analysis of the losses of the power transistor technology used and justifies the choice with respect to the alternatives A first contact with the state plane technique can be had in the description of the power transistors control mechanism The control electronics principle and the inductor specifications are also given here

Chapter 3 makes a mathematical analysis of the equivalent circuit of the generator to show how the state plane analysis technique can be adapted in order to arrive at the steady-state operation condition of the induction generator through a simple construction This approach involves considering a different state than in the traditional approach The construction is defined for all operation modes and control schemes encountered in this generator structure

In chapter 4, a number of examples are given to show that the technique presented in chapter 3 is not limited to establishing the steady-state condition of the generator It aims to show that the technique may be used to observe the behaviour of the power circuit and to explain some of its characteristics These examples are not exhaustive but have been chosen in order to show the range of analysis possibilities of the technique As far as possible they are presented in order of increasing difficulty to allow a gradual exposure to the principles involved

The analyses of the prior chapters are carried out assuming a good knowledge of the generator load In chapter 5, a load measurement method is presented that allows the verification of the theory elaborated in the previous chapters This technique consists of analysing the load current and voltage wave forms in order to extract the impedance information from them It was necessary to develop this technique because no simple alternative exists for a valid measurement and any modelling techniques are not practical for this purpose

1 INTRODUCTION

1 1 Induction heating

The principle of induction heating is well known in industry, where it finds applications as diverse as metal smelting [1] and sterilisation of bottle caps [2] or surface treatment of mechanical parts [3] and sealing of yoghurt tubs [4] In spite of the diversity, each of these applications has the following common points

1 A metallic workpiece which has to be heated to a greater or lesser degree in a given zone or globally according to the application
2 An inductor which is a coil whose shape is adapted to the workpiece so that an alternating current flowing in it will induce a magnetic field and hence eddy currents in a well defined part of the workpiece
3 A generator which produces alternating current at a frequency and power level calculated to enhance the desired effect The combination of the inductor coupled to it's workpiece constitutes the electrical "load" of this generator

When the inductor is in presence of a workpiece, it can be compared to a transformer with a substantial air gap The coil in question is the primary of the transformer and the workpiece is simultaneously the magnetic circuit and the secondary of the transformer The literature in general [1] [2] [3] [5] [6] [7] [8] [9] agrees on the series *RL* combination as a correct equivalent circuit for the induction load The impedance of this combination will vary with the workpiece material and its size and position

1 2 Induction cooking

In the case of induction cooking, the inductor is flat and spirally wound and it is separated from the workpiece, a cooking utensil, by an insulating plate made of a glass-ceramic compound ("VITROCERAMIC") as in Fig 1 1 For many years the numerous advantages of induction heating made cooking an obvious application [10] but the generators proposed were impractical or too costly as revealed in the historical recap of [7] Since the early 70's, RF generators for this application have been receiving increasing attention in the literature The exploitation of power switching techniques has allowed the development of cost-effective, flexible induction hobs in the range from 1 to 6 kW, at first using thyristors and then later transistors The majority of these

generators have been based on the half or full-bridge series resonant converter (SRC) [5] [6] [7] [11] [12]

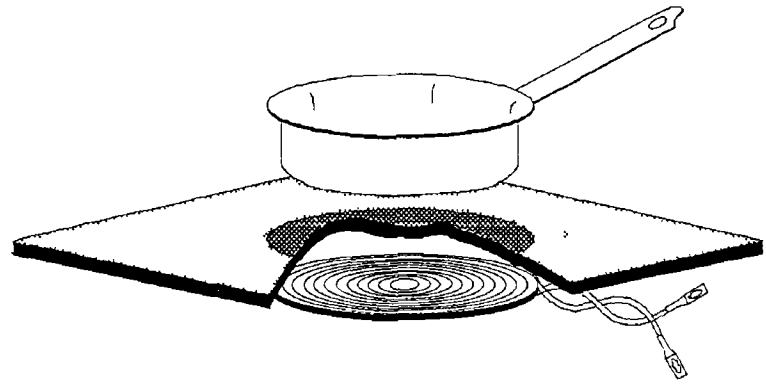

Figure 1 1 Induction cooking generator load

The design of these circuits has been carried out for the most part in a somewhat empirical manner Measurements or analyses have been carried out on a certain number of existing loads and the circuit stresses, and therefore the components, have been defined on these bases This is a hazardous approach since the operating point of resonant converters is dependant on the impedance of their resonant circuit and this impedance is defined by the combination of the inductor and it's workpiece (in this case a cooking utensil) So the workpiece shape, size, material and position play a capital role in the operating point of the converter

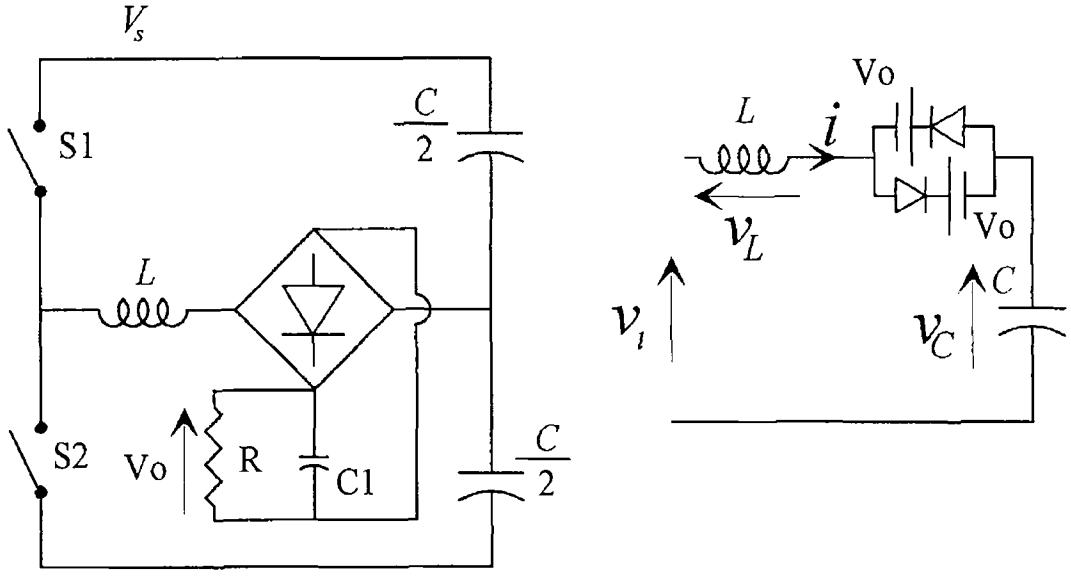

Figure 1 2 Power supply SRC and equivalent circuit

Considering the number of different materials encountered in cookware [13] (cast iron, soft iron, magnetic and non-magnetic stainless steel, copper and aluminium) and the number of utensil diameters and possible positions relative to the inductor, without

mentioning the combination of materials [14] in order to enhance certain properties or the different alloys of stainless steel, it is obvious that the empirical approach is not ideal for design of induction generators

1 3 Series Resonant Converter (SRC)

This structure is well documented in the power supply domain [15] [16] [17] [18] [19] [20] [21] [22]

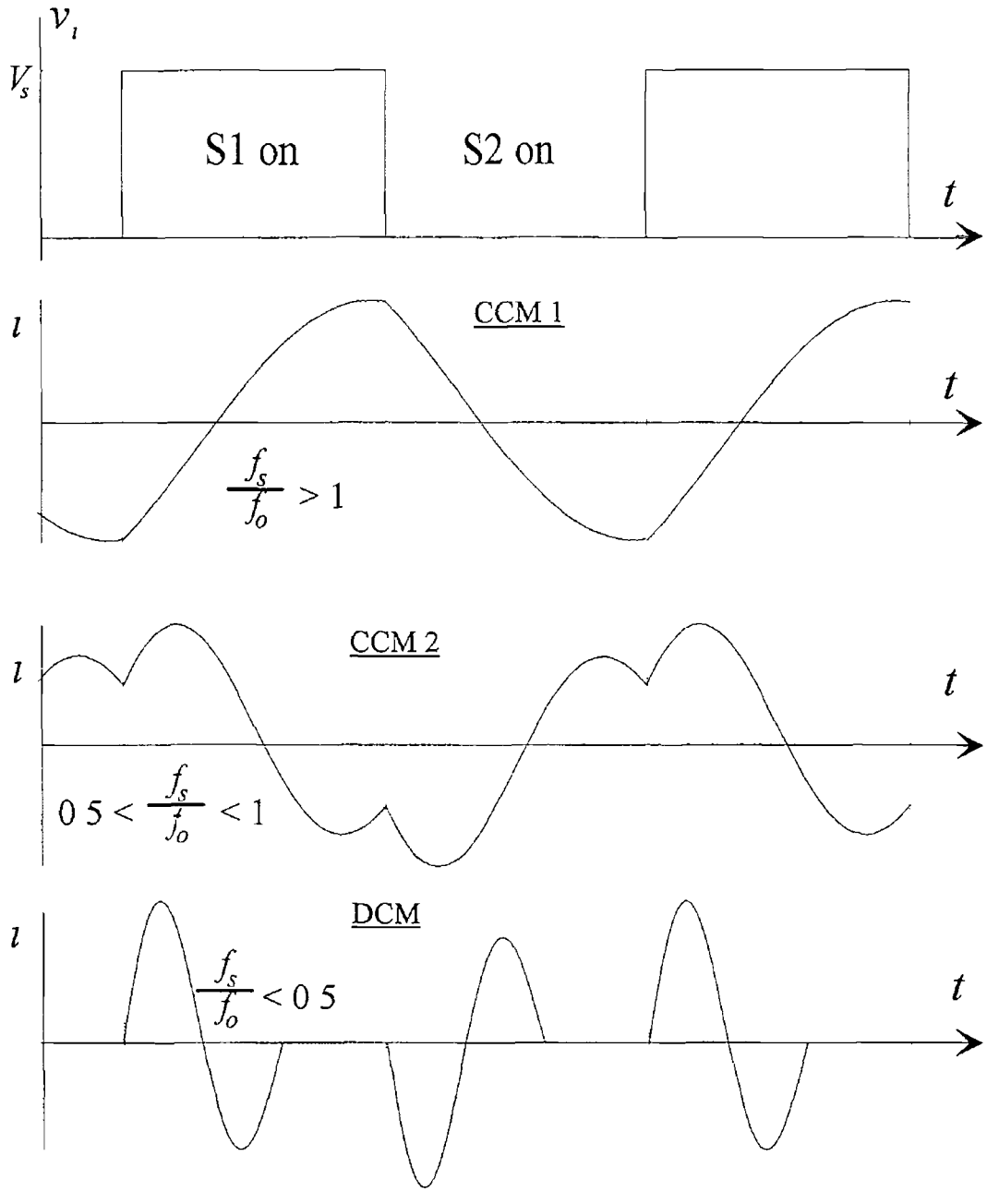

Figure 1 3 Power supply SRC wave forms for various working modes

A simple form of the circuit diagram and its equivalent circuit are given in Fig 1 2 V_s is a d c voltage and the two switches operate in complementary mode Their switching applies a voltage square-wave causing ringing currents in the tank circuit and these are rectified by the diode bridge to give a d c output voltage, Vo Vo can be controlled through the switching frequency The capacitor is divided into two parts connected as shown to reduce peak supply current

[15] describes the SRC's modes of operation in terms of their switching frequency, f_S, with respect to the resonant frequency, f_O, of the tank circuit An infinite number of these exist and [16] groups them into two main categories (Fig 1 3)

a) Continuous Conduction Mode (CCM) In this case the resonant current flows continuously for the full switching period Two types of this mode are reported

CCM 1 $\quad \frac{f_s}{f_o} > 1$

CCM 2 $\quad 0\,5 < \frac{f_s}{f_o} < 1$

b) Discontinuous Conduction Mode (DCM) This occurs when the load current is sufficiently small that the output capacitor need only be charged for a portion of the switching cycle to maintain the steady-state output voltage Thus even though the switch S1 or S2 is closed and capable of conduction, the output diodes become reverse biased, so no resonant current flows in the tank circuit during a portion of the switching period DCM mode is restricted to the frequency range

$$\frac{f_s}{f_o} < 0\,5$$

The literature is unanimous referring to the difficulty of analysing the steady-state operation of the SRC Of course, computer based simulations are possible with a variety of programs available on the market These give excellent results but they are still quite slow in their analysis of the basic power circuits [23] in the realm of resonant converters

Vorperian et al [24] give the first complete solution for the dc conversion ratio, $M = \frac{2Vo}{V_s}$, of the SRC, plotting it against switching frequency for constant values of load resistance However this approach necessitates a new solution to be calculated by iteration each time a circuit parameter is changed Other analytical approaches have been carried out using iteration [18] or Fourier analysis [22], but the result is complex and lacks physical insight into the overall design Apparently, in the field of graphical determination of steady-state operation, two major schools of thought exist

- Output plane
- State plane

1 3 1 Output plane

[15] proposes an analysis based on the expressions derived for the conversion ratio, $M = \frac{2Vo}{V_S}$, in [24] With a change of variable, an explicit expression for M in terms of output voltage and switching frequency is derived From this expression, it is shown that the contours of constant switching frequency are ellipses in the output-plane, I_{out}/M Using these contours, the operating point of the generator can be found in a manner similar to the load line technique

1 3 2 State plane

The state plane representation of the operation of switched series LC circuits is well known in the literature [17] [19] [20] [25] [26] It involves the elimination of the time parameter in the circuit equations and the plotting of the locus of the current versus the capacitor or inductor voltage

It is useful, at this stage to define a convention for referring to the various loci that can be observed throughout this work It is unnecessary to refer to the ordinate variable since it is invariably the current So a valid convention to use is "v_L locus" in order to refer to "the locus that i describes with respect to v_L" This convention will be used throughout this thesis

For the circuit shown in Fig 1 2, on elimination of the time parameter, the circuit equations become

$$\frac{di}{dv_L} = -\frac{C}{L}\frac{v_L}{i} \qquad (1\ 1)$$

$$\frac{di}{dv_c} = \frac{C}{L}\frac{v_i - v_C \pm Vo}{i} \qquad (1\ 2)$$

$\pm$Vo signifies the dependency of the polarity of this voltage on the direction of the current, i The solution of these equations gives arcs of circles in the $\frac{v}{\omega_0 L}/i$-plane with the v_L locus turning anti-clockwise and the v_C locus clockwise

Appealing to symmetry and the fact that all steady-state trajectories are closed, the operating point of the circuit can be easily found for given control and load conditions as shown in Fig 1 4 for the circuit shown in Fig 1 2 From Fig 1 4, it can also be seen that the current and voltage wave forms are always arcs of sinusoids at the resonant frequency of the system and a change in switching frequency only changes the initial conditions of these arcs In short, by allowing the steady-state trajectories to be found in this manner, the use of the state plane transforms a system of sequential differential equations into a problem of simple geometric construction

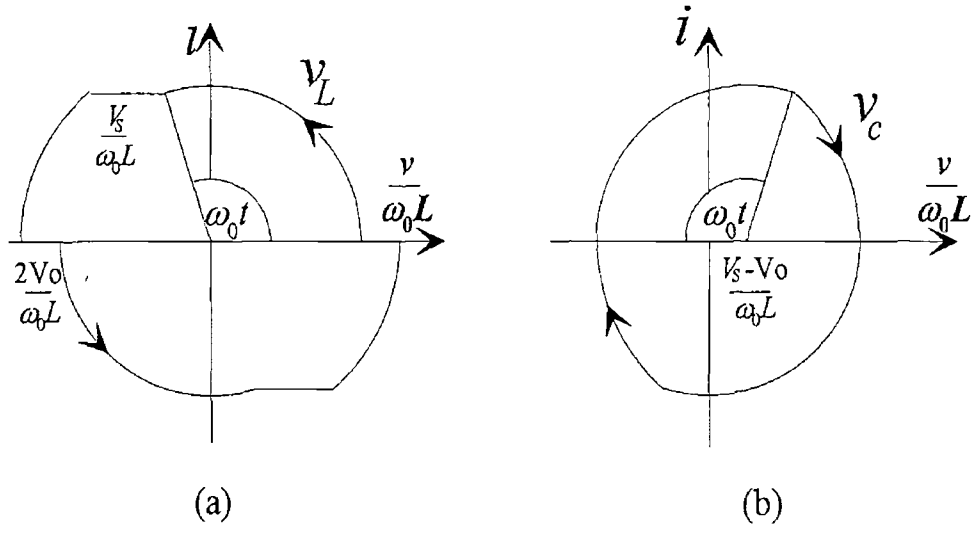

Figure 1 4 State plane plots of (a) v_L and (b) v_C for power supply SRC

The use of the state plane in the analysis of switched low-loss resonant circuits can be found as far back as 1976 [26], applied to television scanning and power supply circuits In this case the states considered were the voltage across the inductive element, v_L and the current i The interest in the state v_L is due to the fact that switching is translated as discontinuities parallel to the voltage axis of a magnitude equal to the switched voltage (Fig 1 4(a)) The corresponding switching points in the v_C trajectory can be seen as discontinuities in the slope of the trajectory This occurs because the centre of the arc of a circle being described is shifted along the horizontal axis by a magnitude equal to that of the switched voltage Another point of interest highlighted is the fact that, in this representation, the angular velocity of the vector describing the trajectory is equal to the natural angular velocity of the resonant circuit, ω_0, such that

$$\omega_0 = \frac{1}{\sqrt{LC}} \qquad (1\ 3)$$

In more recent years, a normalised state plane is applied to the SRC to allow construction of the steady-state trajectory [20] In this case the state that is used is the voltage on the resonant capacitor, v_C This approach is adopted generally [17] [19] The didactic qualities of the state plane are also exploited in [17] in order to demonstrate the different operation modes possible for an SRC An effort was made to extend this technique to resonant circuits with losses [25] The result is an approximation of a semi-spiral function by an eccentric circle that is valid at the end of a half cycle and only for lowly damped circuits

1 4 SRC in induction

The SRC seems to have gained unanimous approval for induction cooking applications as opposed to the industrial domain where the parallel LC structure with a current source supply can also be found Connecting the induction load described in section 1 1 in an SRC will give the circuit and equivalent circuit shown in Fig 1 5 However, the particularities of this circuit with respect to the more traditional power supply circuit give rise to the fact that it is impossible to apply the aforementioned graphical analysis techniques directly This is borne out by the literature [1] [5] [6] [7] [8] [11] [12] [19] where the few analysis techniques used are restricted to Fourier analysis [1] [8], or sine-wave approximation [11] An example exists of steady-state analysis [5] for the case of control through the switching frequency by imposing steady-state conditions on the system equations, but this can not be extended to other control schemes and remains complex and lacking insight

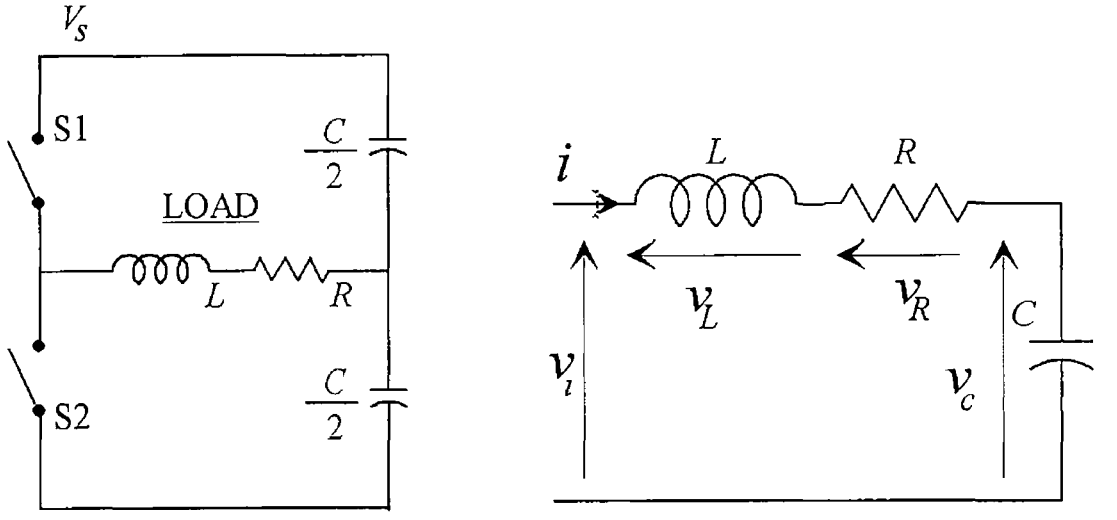

Figure 1 5 Induction SRC and its equivalent circuit

A recap of vector representation of sinusoidally driven RLC circuits is given in [19] but this is only applicable at frequencies near the resonant frequency The fact is that the presence of the load resistance directly in the resonant circuit, instead of being decoupled through a rectifying bridge and smoothing element, gives rise to a number of problems

- State plane analysis of this circuit involves the solution of the following system equations

$$\frac{di}{dv_L} = -C\frac{v_L}{RCv_L + Li} \qquad (1\ 4)$$

$$\frac{di}{dv_C} = \frac{C}{L}\left(\frac{v_i - v_c}{i} - R\right) \qquad (1\ 5)$$

which do not have analytical solutions

- The circuit in question is damped, so the circuit wave forms are no longer sinusoidal but have significant damping This means that the trajectories in the state plane are no longer arcs of circles but arcs of distorted spirals, which renders any graphical analysis difficult
- Every different utensil will give rise to a new RL combination, which in turn will modify the global impedance of the circuit and its resonant frequency This contrasts with the power supply where the unique resonant frequency was defined by the unvarying values of L and C and it was possible to normalise the switching frequency, f_S, with respect to the resonant frequency, f_O, and all voltages with respect to the maximum voltage A contrast also exists in the fact that the conduction time of a switch can no longer be associated with a unique conduction angle as in the power supply This is due to the fact that the natural angular velocity of the circuit changes with the impedance
- The induction load parameters are also inaccessible so analysis using the output-plane is excluded

The induction applications mentioned above are equally divided between CCM 1 [5] [6] [8] and CCM 2 [1] [7] [11] operation DCM operation does not exist in this type of circuit and low power operation generally involves alternating periods of operation at the minimum continuous power level with pauses at a given duty cycle in order to reach low power levels The inertia of the load will cause an averaging of the power that will be imperceptible to the user if the periodic time of this mode is carefully chosen
The Q values of the resonant circuit vary from 2 to 10 At the minimum Q value, power can be adjusted in a range from 10 to 100% by varying the switching frequency In the upper Q values, frequency control can be used to limit the current in the switches

1 5 Load measurement

The determination of the impedance of an inductor-workpiece combination, at a given frequency, has long been at the centre of attention of the literature [1] [3] [5] [6] [10] [11] [13] [14] [27] [28] [29] [30] [31] [32] [33] The task is more difficult than it may seem In order to know the impedance, it is necessary to determine the natural

frequency at which the circuit will oscillate To do this it is necessary to know the impedance The phenomena that determine the impedance in question are

1 Skin effect in the workpiece due to a wide range of frequencies
2 Skin effect and proximity effect in the inductor
3 Saturation of the workpiece material
4 Hysteresis in the workpiece material
5 Variation of the workpiece materials resistivity and permeability with temperature
6 Variety of workpiece materials, geometry, and position with respect to the inductor (particularly in the case of induction hobs)
7 Modification of impedance by a variety of shielding techniques which are destined to reduce electro-magnetic radiation from the inductor onto the circuit or into the air (e g ferrite plates on the lower surface of the inductor, conducting plate surrounding the inductor)

Gaspard shows in [33] that hysteresis and saturation are not encountered in induction hob loads The existing possibilities are theoretical analyses or measurement Among the former are analytical [28] [29] or numerical techniques based on finite elements [5] [10] [13] [14] [30] [31] [33] or surface integrals [32] To take into account the frequency dependence of the impedance, this type of analysis must involve iterative calculations [10] The iterative nature of these calculations can give rise to convergence problems, and the precision of the result must be considered very carefully knowing that for certain iterative systems a small error encountered early on can have a cumulative effect and give a significant error in the result It is also necessary to have the permeability and resistivity characteristics of the material in question For this reason, this type of analysis is not suited to determining the impedance of a large range of utensils It comes into its own in the design of the inductor in order to optimise it with respect to a given utensil, with a minimum of prototypes This is more so the case since inductors are inclined to become combinations of concentric windings [10] to meet the electromagnetic interference norms while still accepting a wide range of utensil sizes
The measurement can be carried out with an RLC-bridge at the appropriate frequency or using a pulse method [11] [27] [32] The existing measurement techniques suffer from difficulties in measuring thermal effects [27] suggests methods of getting around this by substitution of materials or measurements on hot workpieces, but these are hardly practical

2 THE INDUCTION HOB

2 1 Introduction

An induction hob comprises 5 elements

- A **power part**, including mains filtering, rectifier and inverter
- An **inductor**
- The **control electronics** which includes an auxiliary power supply
- A **user interface** to allow the selection of power levels and cooking times
- The four preceding elements are assembled in a **housing** designed to respect various safety, electro-magnetic compatibility (EMC) and hygiene standards

In this thesis, two distinct induction hobs will be considered They are both based on the same basic principle but have been adapted to two different environments These two environments can be resumed as follows

- **Professional** this includes all kitchens where large quantities of meals are produced - hostels, restaurants, hotels, etc This environment is characterised by the necessity of high power delivery, long working duration, extreme climatic conditions (high humidity and temperatures up to 80° C) and the necessity of fine adjustment in the power control over the full range of power The three phase mains is always available and this is used to good advantage in order to supply the high power needed There are no particular constraints on the dimensions of the hob nor on the acoustic noise generated by it
- **Consumer** this refers to the household kitchen where the power is significantly lower, the working duration shorter, the climatic conditions less extreme and the precision of power adjustment less exacting The single phase supply is the only certainty from the mains supply point of view The real constraints of this environment are the level of acoustic noise (due to ventilation for example) and the overall dimensions of the hob All ambient noise due to the hob must be kept to a minimum The hob must comply to a standard in width and length in order that it be possible to incorporate it in a kitchen top and its height must be kept a minimum As with all consumer appliances, low cost is of primary importance

In the hobs in question, the same basic principle of power and control have been used with the necessary adaptations to each environment being carried out on the inductor, the user interface, and the housing A block diagram of the basic structure can be seen in Fig 2 1 for the professional hob and Fig 2 2 for the consumer hob

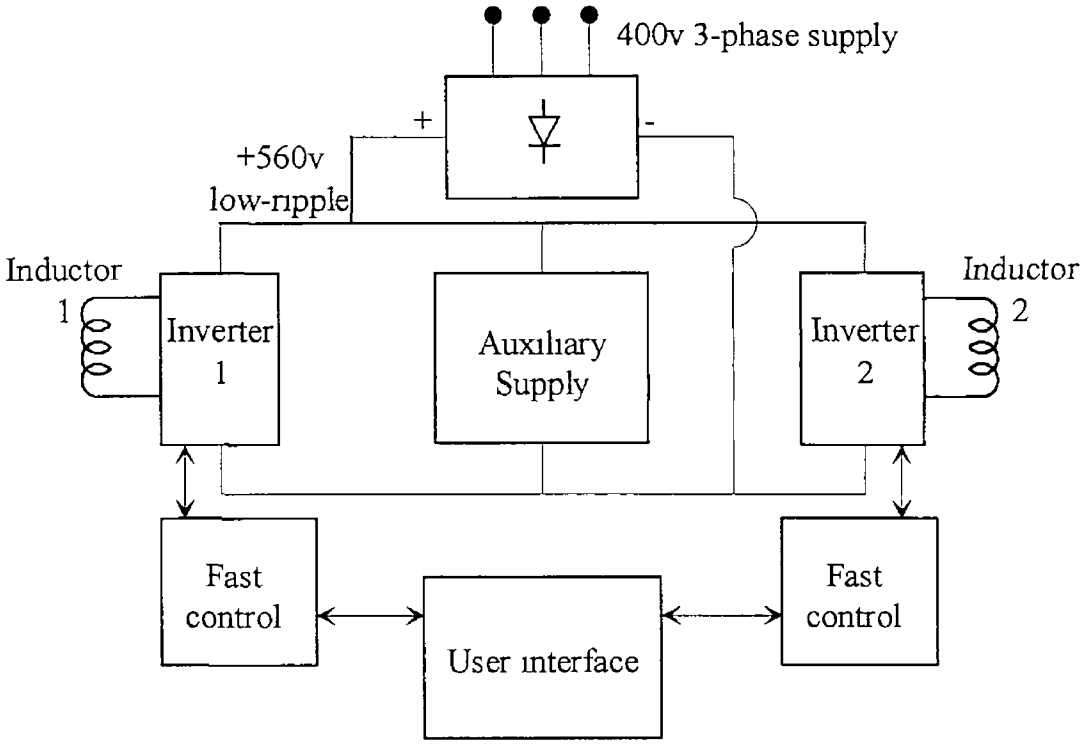

Figure 2 1 Block diagram of professional hob

The professional hob works with two separate inverters, one for each inductor The consumer hob uses the same inverter to supply two inductors through time sharing The distribution is carried out using relays

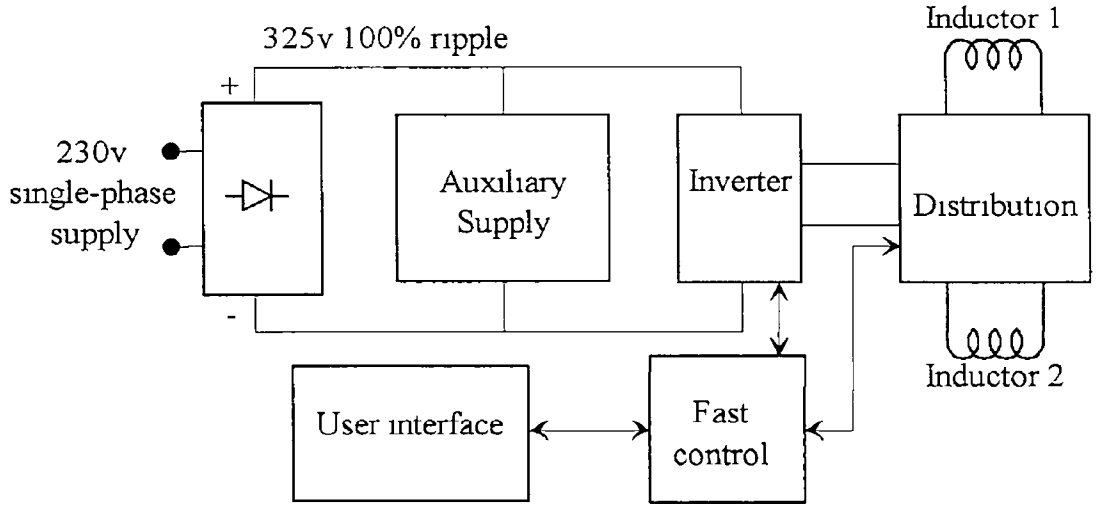

Figure 2 2 Block diagram of consumer hob

The induction hob application is one that has extremely exacting exigencies on the power electronics compared to the typical industrial applications of induction heating and this in spite of what is a relatively low power One of the fundamental difficulties that an induction hob encounters is the fact that the load is "unknown" at start-up while m industrial applications, the load is always of a specific repetitive nature for which the generator and inductor have been designed The next major difference between the two types of application is that the user of an induction hob needs to be able to program power settings freely while the industrial application is kept at constant power or varies according to a predetermined pattern (e g in metal smelting the impedance encountered when the inductor is in presence of molten metal is not the same as that for solid metal but the variation that takes place is well known so it can be predicted) The industrial application is less critical from the safety point of view since the load is often transported automatically without direct human intervention It is not rare to see inductors that have no electrical insulation with respect to the load, apart from clearance in the air This would be unthinkable in the case of an induction hob and it renders the detection of a load all the more difficult

In short, from the numerous constraints imposed by the cooking environment, the following should be emphasised

- Reasonably high power consumption (at least several kilowatts)
- Wide range of power (1 to 100%)
- Fine adjustment of power
- Automatic limitation of power according to size, position and material of utensil
- "no-load" functioning, and detection of any rapid load transitions
- Protection against undesirable loads (i e when pot is aluminium, copper, or certain alloys of stainless steel)

2 2 The power part

2 2 1 Mains filtering

The mains filtering is composed of series inductances before the rectifier bridge combined with parallel capacitances before and after for differential-mode rejection Common-mode filtering is provided by compensation-wound inductances before the bridge combined with capacitors connected to earth The professional unit also has a compensated inductance after the bridge

2 2 2 Supply voltage

Due to the high power requirements of the professional user (6 kW per plate), the supply voltage is drawn from the three-phase mains (i e 400 v a c) to give a low-ripple

560 v supply Using the single-phase supply would triple the cost of the output stage [6] The consumer unit which does not need more than 2 8 kW per plate can work off the single-phase supply (230 v a c) This gives a 325 v 100% ripple supply The difference between the two cases gives rise to power switches with different current and voltage ratings A comparison of the rating of these components according to their application reveals the similarity of the constraints in the two cases

Table 2 1 Comparison of power switch ratings according to application

	Professional	Consumer
Max voltage, V_{max} (volts)	800	500
Max current, I_{max} (amps)	40	60
Switching capacity, V_{max} x I_{max} (va)	32000	30000

From Table 2 1 it becomes obvious that, in spite of an apparent difference of the switch ratings on face value, the "switching capacity" is very similar for both A difference of less than 7% can be noted

2 2 3 Generator structure

The basic generator circuit is the SRC discussed in section 1 4 As with all bridge structures, this circuit has the advantage of imposing a peak voltage on the switches that is no greater than the supply voltage The half-bridge also corresponds to the lowest possible silicon surface area in the power output stage and accepts large variations of the output circuit Q-factor [6] This allows a maximum leeway in the possible range of loads

The generator functions in CCM 1 mode (i e $\frac{f_s}{f_o} > 1$) which means the switches switch on spontaneously when the voltage across them goes to zero and switch off at a controlled instant In general, CCM 1 mode is favourable for the switches because they work at their nominal currents (i e full power) at low frequency Knowing that high frequency switching is an additional stress for any switch, it is preferable not to have the maximum current condition at maximum frequency The power is controlled by varying the switching frequency The load current for three frequency settings can be seen in Fig 2 3 At high frequency in CCM 1 mode, the load current, i, is practically triangular As the frequency decreases tending towards the resonant frequency, the current becomes more and more sinusoidal under the resonant effect, and the power increases It can be seen that, as the power increases, the switched current is no longer equal to the peak current and this fact is exploited to minimise the switching losses for a given power For example, at full power in the professional hob, the current reaches a peak value of 40 A, with a switched current of only 26 A

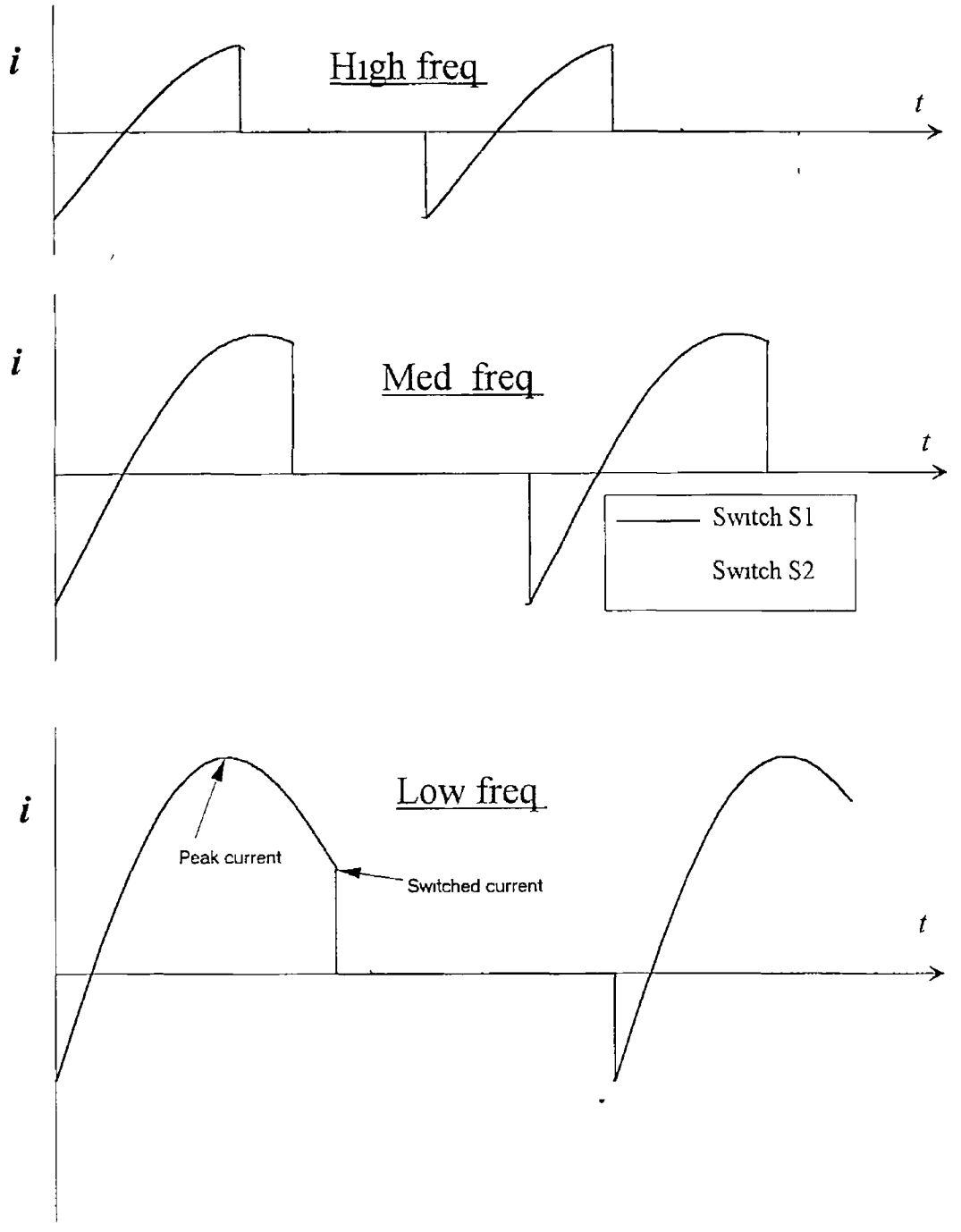

Figure 2 3 Current variations in SRC with frequency

The state plane can be used to visualise the circuits cycle and to understand the effect of frequency variations The three time-domain representations in Fig 2 3 are also represented in the state plane in Fig 2 4 by their v_L locus It can be seen that the surface area enclosed by the trajectory is an indication of the power since it increases with the power from one case to the next It is also possible to analyse the nature of the switches through the state plane as described in [19] [26] As a recap on this aspect of the possibilities of the state plane approach, the analysis of the switches is carried out in the next paragraph

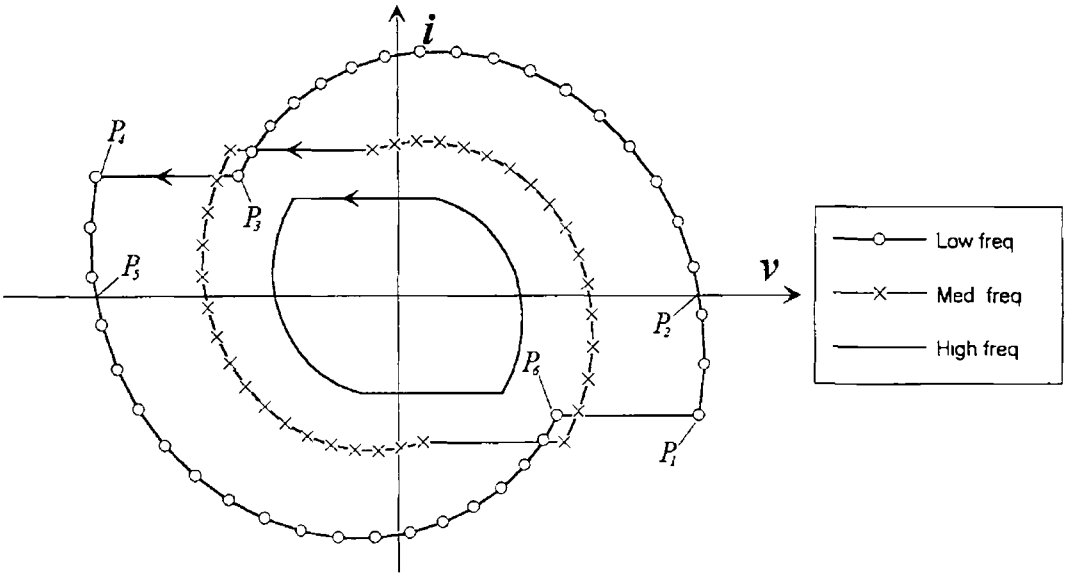

Figure 2 4 State plane representation of v_L locus for frequency cases seen in Fig 2 3

Given the frequencies involved (>20 kHz), the switches in question can only be implemented in reality by semiconductor switches The symmetry of the cycle indicates that they are both identical An examination of Figs 1 5 and 2 4 reveals that S1 conducts from P_1 to P_3 and S2 from P_4 to P_6 From the polarity of the current it is clear that the switches are bi-directional in current and uni-directional in voltage This leads to the use of a transistor with freewheel diode With this structure, since the current is switched by the active switch at P_3 and P_6, the continuity of the current is ensured by the diodes from P_1 to P_2 and from P_4 to P_5 Taking into account these considerations, the final circuit configuration, using bipolar transistors, is shown in Fig 2 5 There are several technologies possible for the implementation of the active switch The choice of bipolar transistors is justified in section 2 3

Switching on or off at zero volts allows the use of non-dissipative switching-aid networks which reduce the switching losses without a loss in overall efficiency For this mode, such a network involves the connection of a capacitor in parallel with each switch as seen in Fig 2 5 This mode also has advantages for mains pollution because the generator wave form tends toward a sine-wave as the power increases This means that at high power, when mains pollution is maximum, the generator wave form will be less rich in high frequency harmonics Since a major part of the mains pollution above 20 kHz comes from these harmonics, the mains filter will not need to be as big as in CCM 2 mode for an equivalent power level The lower frequency harmonics are avoided by working with 100% modulation of the supply voltage This means that the generator appears as a resistive load to the mains supply

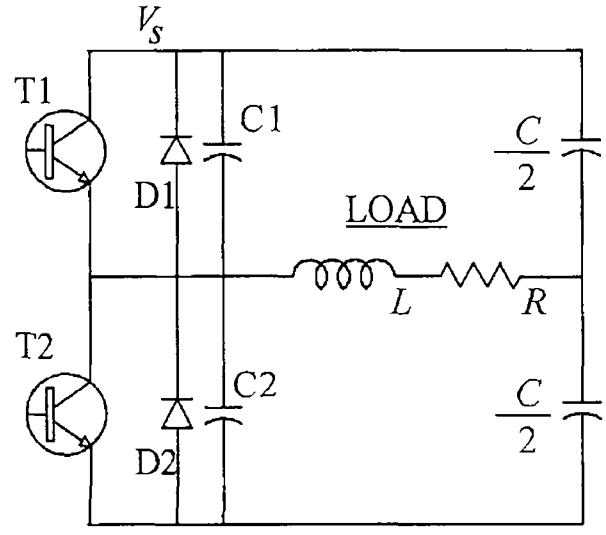

Figure 2 5 SRC for induction heating application

2 2 4 Dimensions

As an indication, the professional power part which includes two 6 kW inverters consists of two boards whose combined dimensions are as follows

Length	390 mm
Width	330 mm
Height	63 mm

The consumer power part, which includes one 2 8 kW inverter, has the following dimensions

Length	210 mm
Width	185 mm
Height	30 mm

2 3 Choice of active power switches

For the SRC working at frequencies greater than the resonant frequency to supply 2 8 kW from a rectified 230 volt mains supply with 100% modulation, the power switch must withstand 500 volts and a peak current of 60 amps Three possible power switch technologies can be envisaged

- Bipolar Junction Transistor (BJT)
- Metal Oxyde Semiconductor Field Effect Transistor (MOSFET)
- Insulated Gate Bipolar Transistor (IGBT)

The latter two have the advantage of being relatively simple to control as compared to the former However, this can not be an adequate reason for a choice, which should be based on more objective criteria The main criterion for choice of a power switch is its losses in the application The losses condition the size of the heat sinks and the cooling air flow that has to be provided These factors have a major influence on the overall dimensions of the product and on the amount of ambient noise generated by it They are to be kept to a minimum in the case of a consumer product

The exact nature of the losses varies according to the technology of the device In order to carry out a comparative study of the losses, it is necessary to consider the characteristic of each component separately in order to model them in terms of resistances and voltage sources Once these models are established, it will be possible to put values on each element of the models based on data sheets of real components The conduction losses can then be calculated using measured values of r m s and average current In this case the current has been measured at 2 8 kW with a supply of 230 v The load impedances are 3 Ω and 32 µH and the resonant capacitor is 1 36 µF The measurement must be made over at least one half period of the mains cycle in order to account for the mains ripple When more than one half period is taken, a whole number of half periods should be used The values found for each switch were

I_{rms} = 21 A
I_{av} = 11 4 A

2 3 1 BJT

Referring to the characteristic of the BJT in Fig 2 6, we see that it behaves

- like a resistance, R_{on}, in it's saturation zone
- more or less like a current source in it's linear zone

In order for the device to operate in it's saturation zone, a sufficiently high base current must be supplied The value of this base current is defined by the "forced gain", β_f, and the value of the collector current I_c [34] R_{on} can be calculated as follows

$$R_{on} = \frac{V_{ce(sat)}}{I_{c(sat)}} \qquad (2\ 1)$$

The conduction losses in the base of the BJT must also be considered The model for the base is similar to that of a diode with a threshold voltage of 0 7 volts and a series resistance R_{be}, defined as

$$R_{be} = \frac{V_{be(sat)} - 0\ 7}{I_{b(sat)}} \qquad (2\ 2)$$

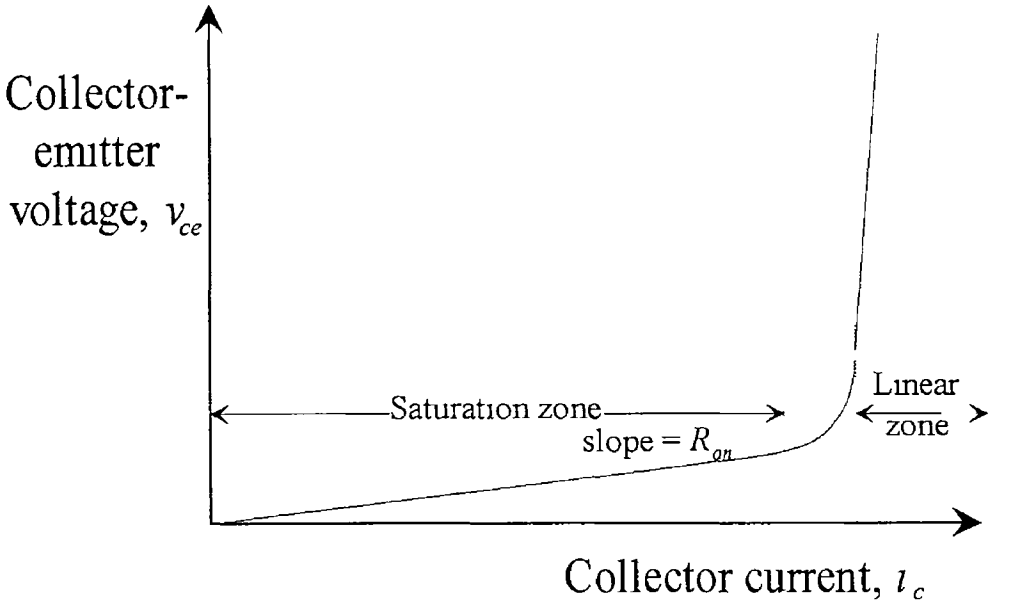

Figure 2 6 Characteristic of BJT

The total conduction losses are then given by

$$L_C = R_{on} I_{rms}^2 + R_{be} \left(\frac{I_{rms}}{\beta_f} \right)^2 + 0\,7 \frac{I_{av}}{\beta_f} \qquad (2\,3)$$

The BUT 92 ITH has a V_{ces} of 500 volts and a V_{ceo} of 250 volts It has a $V_{ce(sat)}$ of 1 3 volts at 60 amps and a $V_{be(sat)}$ of 1 3 volts at 3 amps Substituting above gives

$$R_{on} = 0\,022\ \Omega$$
$$R_{be} = 0\,2\ \Omega$$

With a β_f of 5 these values give conduction losses of 14 8 watts for the extreme case The measured losses of a typical case (in the conditions defined above) are found to be 15 watts, confirming that the conduction losses are a significant part of overall losses

2 3 2 MOSFET

In practice, the switching losses of the MOSFET can be ignored

The conduction losses, L_C, can be defined as those of its drain-source resistance in the "on" state, R_{on} (refer to the characteristic of Fig 2 7)

$$L_C = R_{on} I_{rms}^2 \qquad (2\,4)$$

In order to achieve the overall losses desired, a number of MOSFET's can be connected in parallel This is rendered possible by the simplicity of their control To achieve the level of losses set by the BJT, the conduction losses, L_C, of the MOSFET must be equal to the total losses of the BJT, i e 15 watts Substituting for L_C and I_{rms} in (2 4) gives the necessary value of R_{on} This value is 0 034 Ω A typical 500 v MOSFET in a TO-

218AC package has a resistance of 0 55 Ω at 4 A (junction temperature 100° C), which means that we need 16 devices in parallel to achieve the desired resistance for one switch The total number of devices per generator will be 32

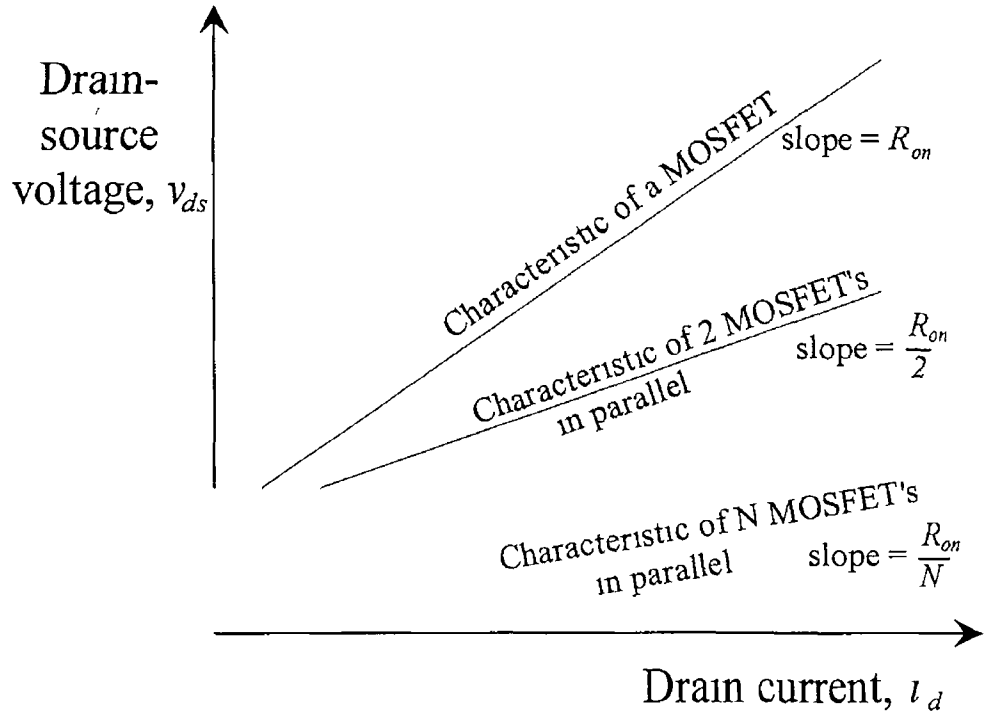

Figure 2 7 MOSFET characteristics

This solution would lead to a serious increase in the surface area of printed circuit board, and would be totally impractical, from an industrial point of view

2 3 3 IGBT

The IGBT switching losses in this case can be considered equal to those of the BJT for the most recent generation of IGBT's called "Ultrafast" An examination of the IGBT characteristic given in fig 2 8 shows that the conduction losses of this device are the sum of those due to its threshold voltage, V_t, and those due to its R_{on} The expression for the total conduction losses [35] is

$$L_C = V_t I_{av} + R_{on} I_{rms}^2 \qquad (2\ 5)$$

The nearest "Ultrafast" IGBT to specification is a 600 volt which has an R_{on} of 0 037 Ω and a V_t of 1 45 volts These values give 32 9 watts of conduction losses The additional losses with respect to the BJT will impose additional cooling

The global losses for such an IGBT in the above-mentioned conditions have been measured at 35 w

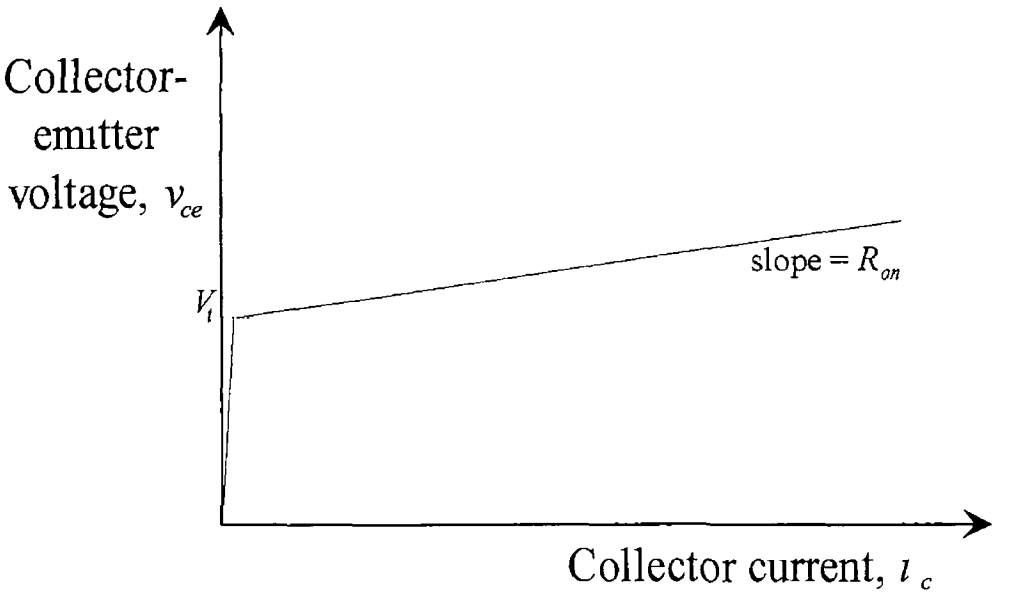

Figure 2 8 Characteristic of IGBT

2 3 4 Conclusions

In order to complete the comparison of the various power switch options, it is necessary to consider the cost of each Table 2 2 gives the relative prices of the switches and their driving circuitry as a percentage of the BJT solution along with the results of the loss measurements and calculations

Table 2 2 Table of costs and losses for each switch option

	BJT	IGBT	MOSFET
Cost of switches and drive	100 %	83 %	293 %
Conduction losses for the two switches (calculated)	29 6 w	65 8 w	30 w
Total losses for the two switches (measured)	30 w	70 w	*

*No measurement was made on the MOSFET due to the fact that its high price excluded it from any further consideration

The MOSFET can not be considered due to its price At first appraisal the IGBT solution is cheaper However, the calculation and the measurements concord to indicate a serious increase (by a factor of 2 3 for the measured values) in the losses for the IGBT with respect to the BJT The calculations allow the major part of this difference to be attributed to the conduction losses The use of the IGBT's in the induction hob in

question will necessitate an increase in the dimensions of the transistor heat sink and/or an increase in the cooling performance of the fan in order to evacuate the excess calories efficiently It is difficult to appraise the economic consequences of such a modification without a detailed study One thing is certain, the resulting increase in overall dimensions or ambient noise caused by a more powerful cooling fan would be detrimental to the commercial image of the consumer induction hob which has forged itself a place among the upper-range products On the other hand, it is quite possible to imagine IGBT's being used in the professional environment where the noise and space factors are less critical The IGBT is often proclaimed as being a more rugged device, and the professional environment does tend to be more exacting These two facts would seem to reinforce the possibility of seeing professional hobs being marketed with IGBT's It remains to be seen if the ruggedness of the IGBT corresponds to the exigencies of professional use This can only be confirmed by an in-depth study, and mass-production

2 4 Transistor control mechanism

The collector current is of a quasi-sinusoidal shape, and the base current must follow this shape (see section 2 3 1) if the BJT is to stay saturated A current transformer was adopted as a means to achieve this [36] The basic circuit is shown in Fig 2 9

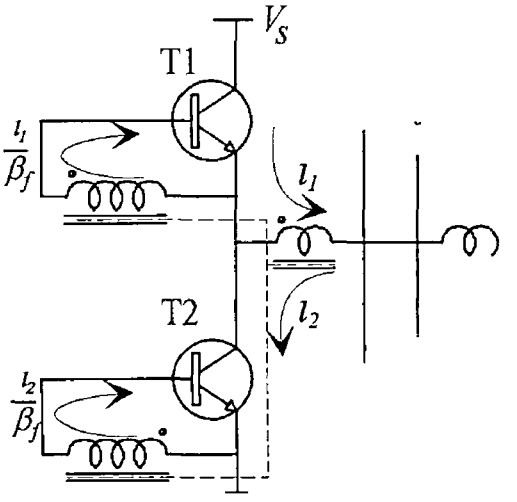

Figure 2 9 Current transformer for base current supply

At switch off, the base current must become negative in order to evacuate the "stored charge" [34] In order to apply a negative voltage to the base, a cell consisting of three diodes in parallel with an electrolytic capacitor is connected in series with each base as shown in Fig 2 10 During the conduction of the transistors, the base current maintains the charge of the electrolytic capacitor at $3V_d$ When the voltage on the base winding of

the current transformer is nullified, a negative voltage of $-3V_d$ (~ -3 v) is applied to the base of the bipolar transistor

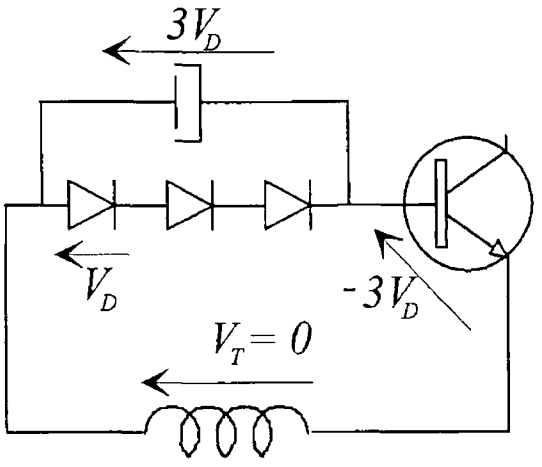

Figure 2 10 Base cell for negative voltage

The voltage of the base winding is brought to zero by short-circuiting a second pair of windings on the same transformer This operation is carried out by switching on the small MOSFET shown in Fig 2 11

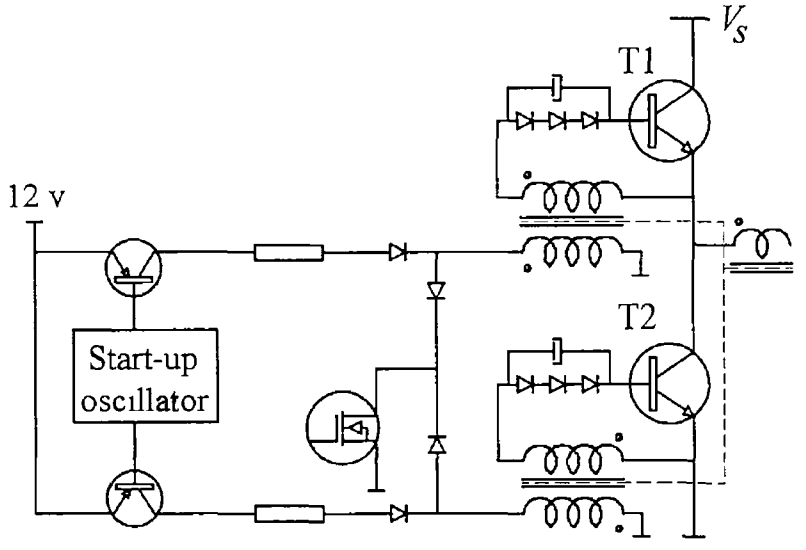

Figure 2 11 Complete base drive circuit

The base current required for start-up is supplied by a small oscillator with two complementary outputs each driving a transistor connected to one of the base windings as shown in Fig 2 11

The current transformer used in this base drive system ensures that the control alternates between the two power transistors at each switch-on instant The mechanism by which this alternance is ensured can be best understood by using a state plane

representation The transformer model, seen from the base circuit side, is a perfect transformer in parallel with a magnetising inductance, L_m, as shown in Fig 2 12

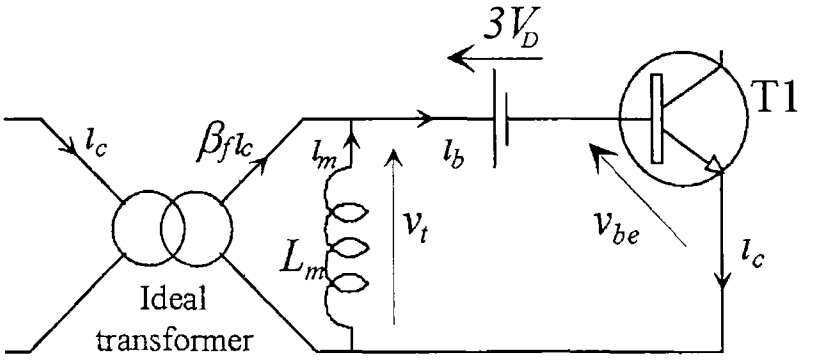

Figure 2 12 Base drive circuit with transformer model

The state plane representation of the voltage v_t and the magnetising current, i_m, are shown in Fig 2 13(a) Fig 2 13(b) shows the steady-state cycle of the v_L locus at a given frequency Supposing the control MOSFET switches off at P_1 From Fig 2 13(a), we see that i_m is positive and continues flowing through the base-collector diode of T1, thus preparing T1 for conduction as soon as D1 switches off at P_2 The inverse effect can be seen at P_5, where the negative i_m ensures that T1 is kept non-conducting up to the transition which happens at P_6

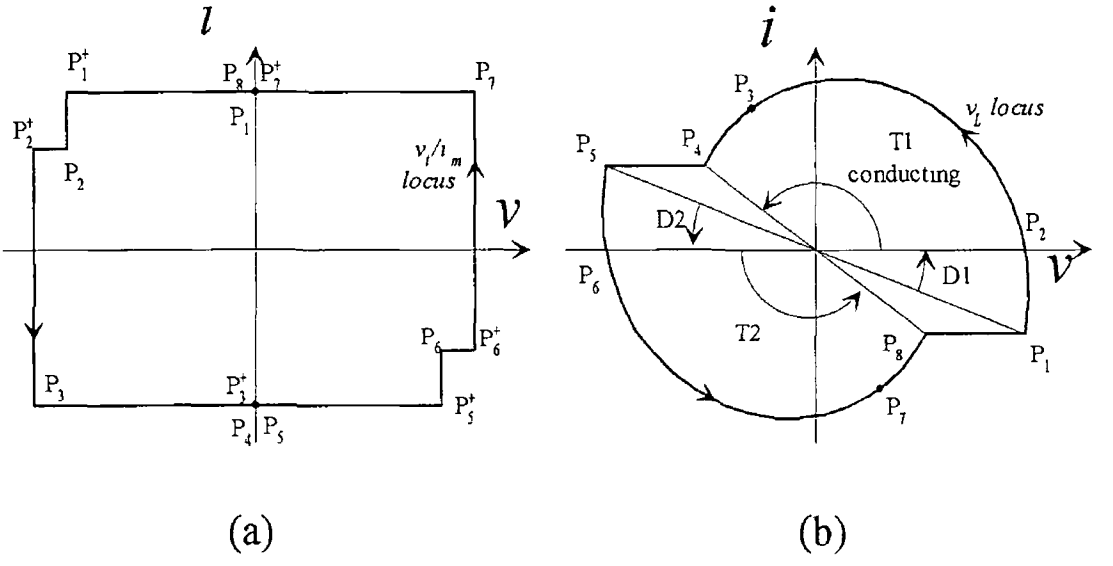

Figure 2 13 State plane representation of the (a) v_t/i_m and (b) v_L loci

It should be noted that

$$\beta_f i_c >> i_m$$

This masks the inversion of i_m during the transistor conduction time

2 5 Control electronics

Power control and current limitation are achieved by varying the switching frequency (see Fig 2 14) This variation is carried out by controlling the transistor "on-time" To accomplish this it is necessary to dispose of a synchronisation that indicates the start of the transistor conduction time This information is drawn from the signal of a second current transformer connected as shown in Fig 2 15 The synchronisation pulse resets a monostable whose time delay is programmable The monostable controls the MOSFET through a driver circuit

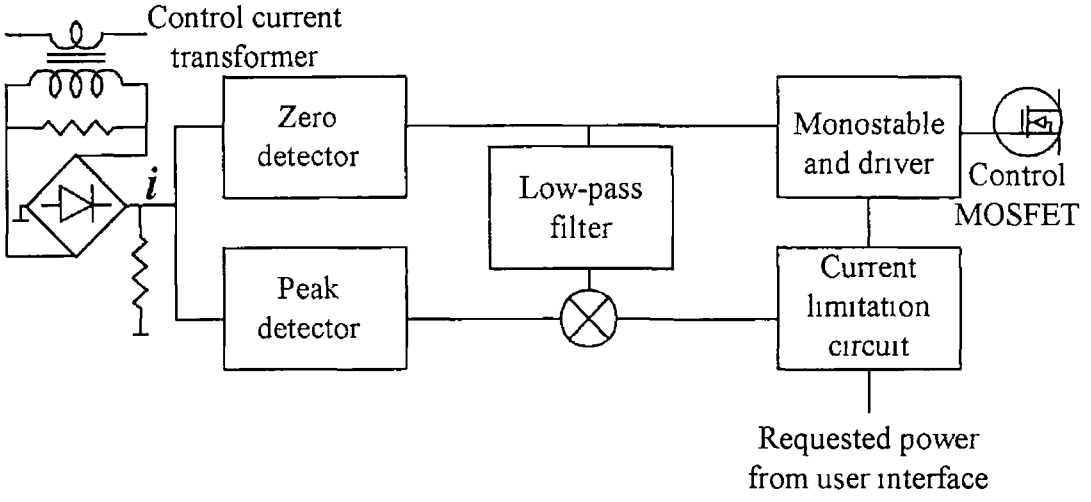

Figure 2 14 Block diagram of power control and switching current limitation

The control part must cater for variations of load in order to limit the switched current to acceptable levels It is also necessary to cater for the case of power being requested in an unsuitable load (copper, aluminium, or non-ferritic stainless steel) or without any utensil (no-load) This function is fulfilled by a circuit whose block diagram is shown in Fig 2 14

The principle of this limitation is explained in detail in [6] and [37] It is a fast control which modulates the "requested" power coming from the user interface according to the different loads encountered This can be achieved because the duty cycle of the transistor conduction time to that of the total switch conduction time is an indication of the nature of the load The second current transformer is placed in such a manner that only the transistor current will flow in it (see Fig 2 15) The zero detection block will form its rectified secondary voltage into a duty cycle wave form which, when filtered, will give a d c level which can be compared to the peak current in order to generate a correction signal for the current limitation circuit This d c level can also be compared to a lower fixed threshold to determine when a load is too small to allow the generator to function This is an important security function to prevent small objects like cutlery from being accidentally heated if they are inadvertently left on the hob This information

can also be used compared to an upper fixed threshold to avoid the generator working too close to the resonant frequency In this case the error message will increase the frequency in the same manner as the current limitation

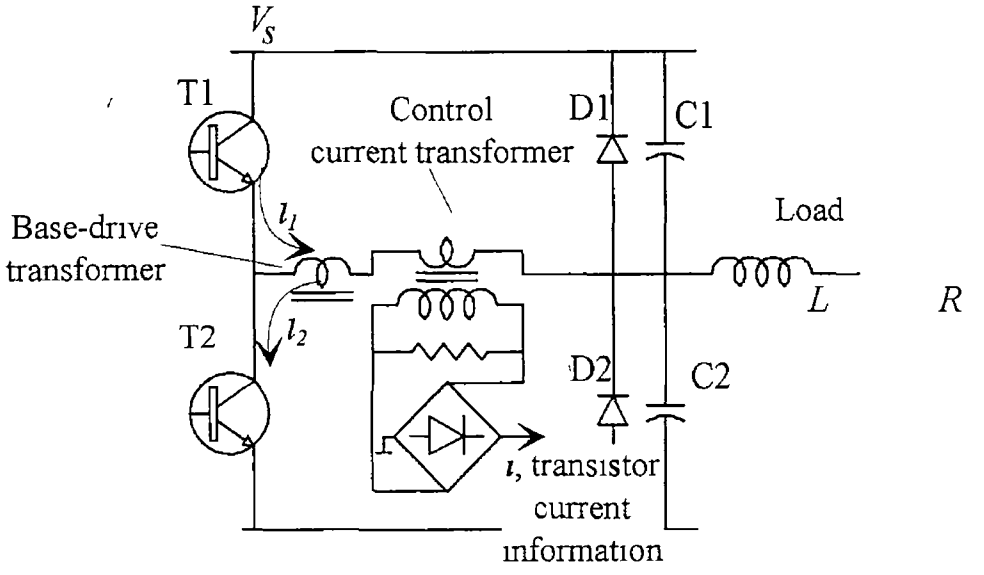

Figure 2 15 Connection of control current transformer

In short, this control circuit carries out a kind of continuous measurement of the Q factor of the load In this manner, it can cater for variations or absence of the utensil and also prevents the inverter from working too close to resonance

Once again as an indication, the professional control part which includes the control for two 6 kW generators and an auxiliary power supply consists of a board whose dimensions are as follows

Length	320 mm
Width	95 mm
Height	25 mm

The consumer control part, which includes the control for one 2 8 kW generator and its auxiliary power supply, has the following dimensions

Length	110 mm
Width	150 mm
Height	20 mm

2 6 Inductor

The inductor will be defined in order to give highest yield in presence of a reference utensil (i e a specific diameter of a specific material) and being driven with a given

supply voltage and resonant capacitor In more traditional induction applications, the inverter is coupled to the inductor with an impedance transformer which allows the use of one inverter of a given power and frequency range to be used for many different inductors This solution is too costly for a product with a large distribution So for the induction hob application the matching transformer function has to be carried out by the inductor In order to decrease self heating due to the skin effect, a braided wire is used The two inductors in question are mounted centred in a hole in an aluminium sheet This serves as electromagnetic screening in order to comply with the relevant norms on radio interference

A drawing of a section through the mechanical arrangement of the professional inductor can be seen in Fig 2 16 The arrangement has rotational symmetry about a vertical axis, so only half of it is shown

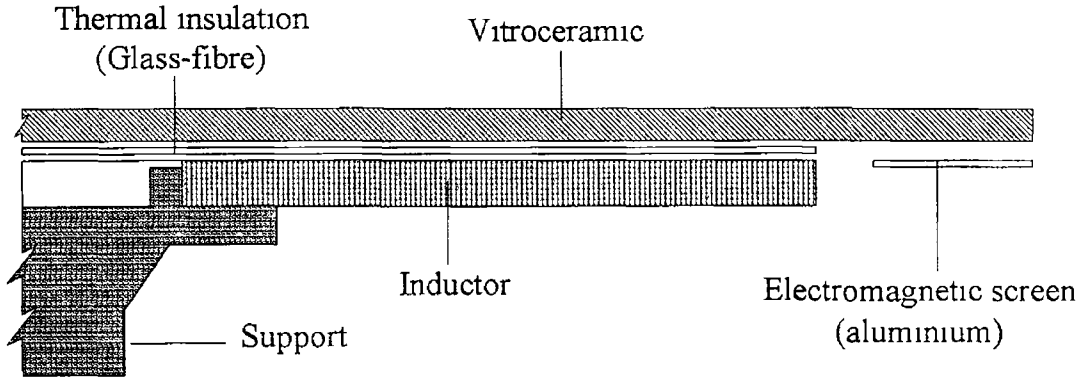

Figure 2 16 Cross-section of professional inductor in position

The professional inductor is wound with 81-strand braided wire formed into a rectangular cross-section of 7 mm by 2 mm The diameter of the individual strands is 0 315 mm It has a total of 47 turns and a diameter of 247 mm

The consumer inductor is wound with 40-strand braided wire on a supporting plate The diameter of the individual strands is 0 4 mm It has a total of 23 turns and a diameter of 185 mm Ferrite plates are attached at intervals on the lower surface of the plate (see Fig 2 17) Their presence improves the coupling with the load and shields the electronic circuits from the electro-magnetic field

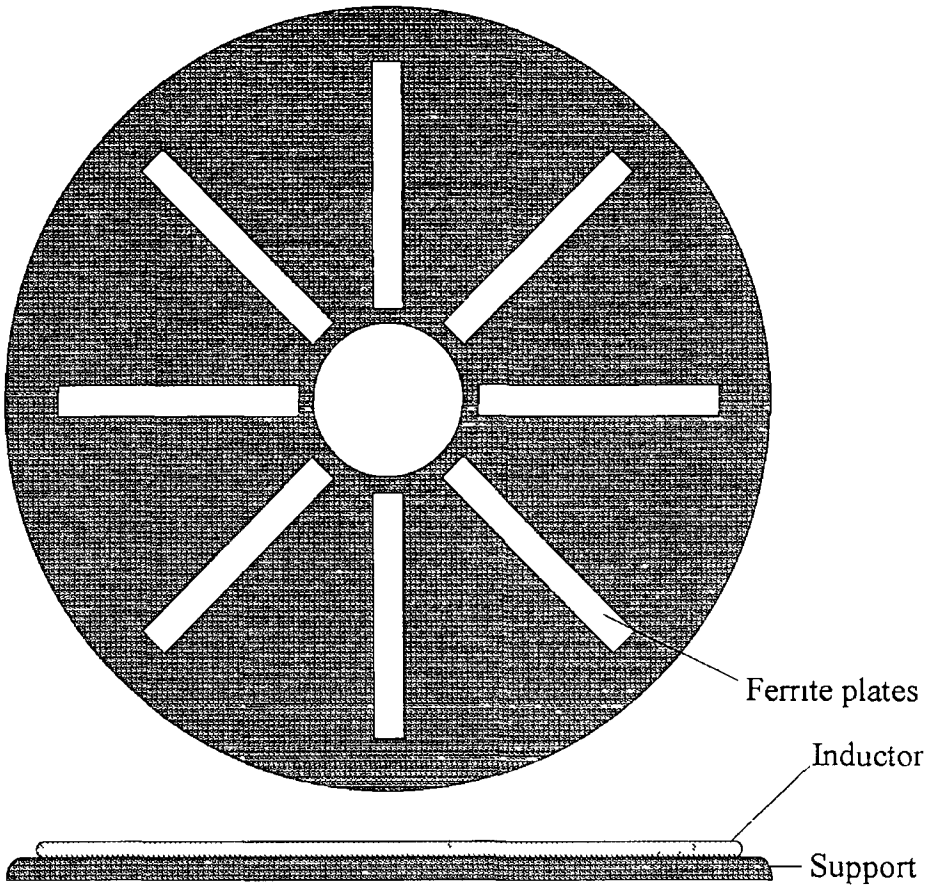

Figure 2 17 Consumer inductor with ferrite plates

2 7 User interface

The professional hob has two fluorescent 6-digit 7-segment displays which allow the display of power level as a percentage of total power with a reduction of the displayed value if the load causes the limitation circuit to be activated The time elapsed is displayed, or if a duration is programmed, the time left to cook is displayed This time can reach 999 minutes There is also a message displayed to indicate when an undesirable utensil is being used

The consumer hob has three buttons to program preselected levels, low medium and high, and a "+" and "-" button to adjust between them over 12 different levels Each level is represented by a light emitting diode A timer up to 99 minutes is also available

2 8 Housing

A variety of housings exist for the professional and consumer hobs, but it is interesting to note the smallest possible outer dimensions for each case The professional unit in question has the following dimensions

Length	800 mm
Width	469 mm
Height	225 mm

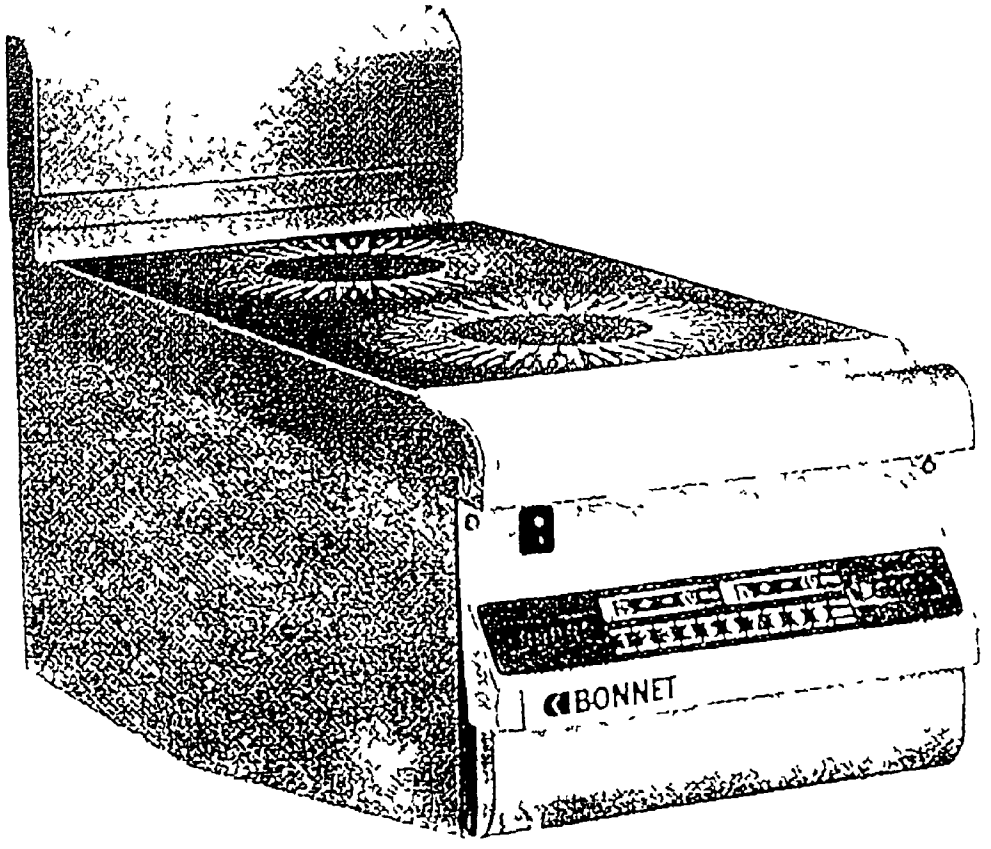

Figure 2 18 Wall mounted professional induction hob

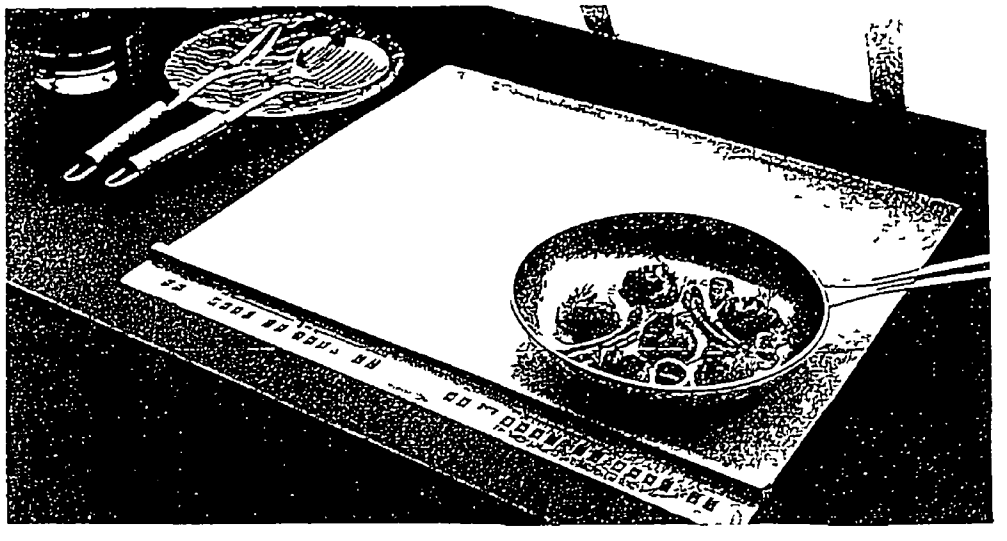

Figure 2 19 Fitted consumer induction hob

A two-plate consumer hob exists with dimensions

Length	510 mm
Width	290 mm
Height	60 mm

A photograph of an example from the existing range of hobs in each denomination is given Figs 2 18 and 2 19

3 STATE PLANE STEADY-STATE ANALYSIS OF INDUCTION SRC

3 1 Introduction

The difference between the traditional SRC for power supply applications and that for induction heating (see section 1 4) imposes a new approach to the SRC analysis problem

The analysis that is to follow is based on the state plane, but differs from the work done in the state plane so far in that it considers damped voltage and current wave forms For completeness, two loci are considered v_L and v_C The parametric equations of these signals are derived for the case of free oscillations With a judicious choice of scaling for the v-axis, two other interesting loci associated with the circuit are brought into evidence A similar scaling already exists in the literature, but it is only applicable to lowly damped circuits, which is not our case The loci revealed in the present analysis are of interest because each one allows the derivation of one of the original loci by a simple transformation They take the form of logarithmic spirals and their properties will be exploited in order to elaborate a graphical technique for establishing the steady-state operation of the SRC in the induction application The analysis is continued on the spiral associated with the v_L locus because the result is easier to follow The case of the v_C locus will be considered later Now, in order to approach a solution for the limit-cycle, a case of forced oscillations with arbitrary initial conditions is considered in the state plane The necessary conditions for steady-state operation are discussed, and a graphical technique for imposing this steady-state condition in the state plane is revealed This is done for the two operation modes encountered in induction (i e switching frequency above and below resonant frequency) Within each of these operation modes, two control schemes differing in the independent variable used as control parameter will be dealt with In the case of switching frequency above resonant frequency, the control parameters are switching frequency and transistor conduction time In the other case, switching frequency and diode conduction time are used

3 2 General solution for free oscillations

The basic circuit in consideration is a series RLC combination as shown in Fig 3 1

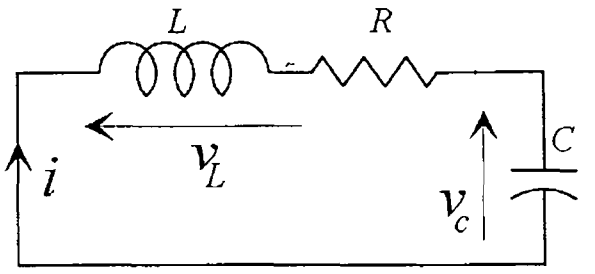

Figure 3 1 Series *RLC* combination in free oscillation

A solution for the system is well known and can be found by solving the following differential equation

$$\frac{d^2 i}{dt^2} + \frac{R}{L}\frac{di}{dt} + \frac{1}{LC} i = 0 \qquad (3\ 1)$$

Consider an anti-clockwise logarithmic spiral, $\bar{s}$, in the complex plane such that

$$\bar{s} = Ae^{-\alpha t} e^{j(\omega t - \gamma)} \qquad (3\ 2)$$

Where $\alpha = \frac{R}{2L}$

$\omega = \sqrt{\omega_0^{\ 2} - \alpha^2}$ $\qquad$ $\omega_0 = \frac{1}{\sqrt{LC}}$

R, L, and C being parameters that are known in the system

Decomposing $\bar{s}$ into imaginary and real parts gives

$$\mathrm{Im}[\bar{s}] = Ae^{-\alpha t} \sin(\omega t - \gamma) = i(t) \qquad (3\ 3)$$

$$\mathrm{Re}[\bar{s}] = Ae^{-\alpha t} \cos(\omega t - \gamma) = \frac{v^*(t)}{\omega L} \qquad (3\ 4)$$

(3 3) is a solution for (3 1)

(3 4) reveals an interesting voltage, $v^*(t)$, which can be expressed in terms of the circuit by

$$v^*(t) = v_L(t) + \frac{R}{2} i(t) \qquad (3\ 5)$$

This means that the spiral, $\bar{s}$, represents $i(t)$ as its ordinate and the voltage, $v^*(t)$, as its abscissa with a scaling factor of $\frac{1}{\omega L}$, which is the admittance of L For convenience, all voltages considered in graphic representations will be normalised to currents with this scaling factor This renders the two axes homogeneous In order to avoid confusion, a capital letter will be used to distinguish these normalised voltages So, for example

$$V^* = \frac{v^*}{\omega L}$$

A similar spiral, clockwise this time, exists in association with $v_C(t)$ Its abscissa, $\frac{v^{**}(t)}{\omega L}$, is given by the expression

$$\frac{v^{**}(t)}{\omega L} = -Ae^{-\alpha t}\cos(\omega t - \gamma) \qquad (3\ 6)$$

$v^{**}(t)$ can be written

$$v^{**}(t) = v_c(t) + \frac{R}{2}i(t) \qquad (3\ 7)$$

The physical significance of v^* and v^{**} can be seen in Fig 3 2

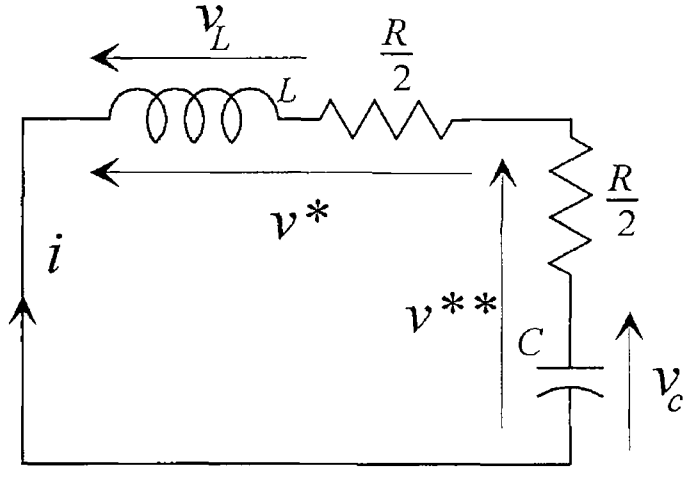

Figure 3 2 Physical significance of v^* and v^{**}

It is, of course, impossible to have access to v^* and v^{**}, just as it is with v_L, but these voltages are extremely useful for the analysis of the circuit due to their properties and the fact that the other wave forms can be derived from them The losses of the circuit have been distributed between the reactive components This result can appear logical with respect to the lossless case since at resonance the impedances of the reactive components are equal

3 2 1 Initial conditions

Let $i(0) = I_0$

$v^*(0) = E_0$

Then

$$\gamma_0 = \tan^{-1}\left|\frac{I_0}{E_0}\right| \qquad (3\ 8)$$

$$A_0 = \sqrt{E_0^2 + I_0^2} \qquad (3\ 9)$$

It can be seen from the expressions for the initial conditions that they take on all their graphical significance in the logarithmic spiral locus (refer to Fig. 3.3). This is also the case for the natural angular velocity, ω, which becomes the angular velocity of the vector that traces the logarithmic spiral locus. These facts will allow the elaboration of the graphical technique to be presented for analysis of the SRC.

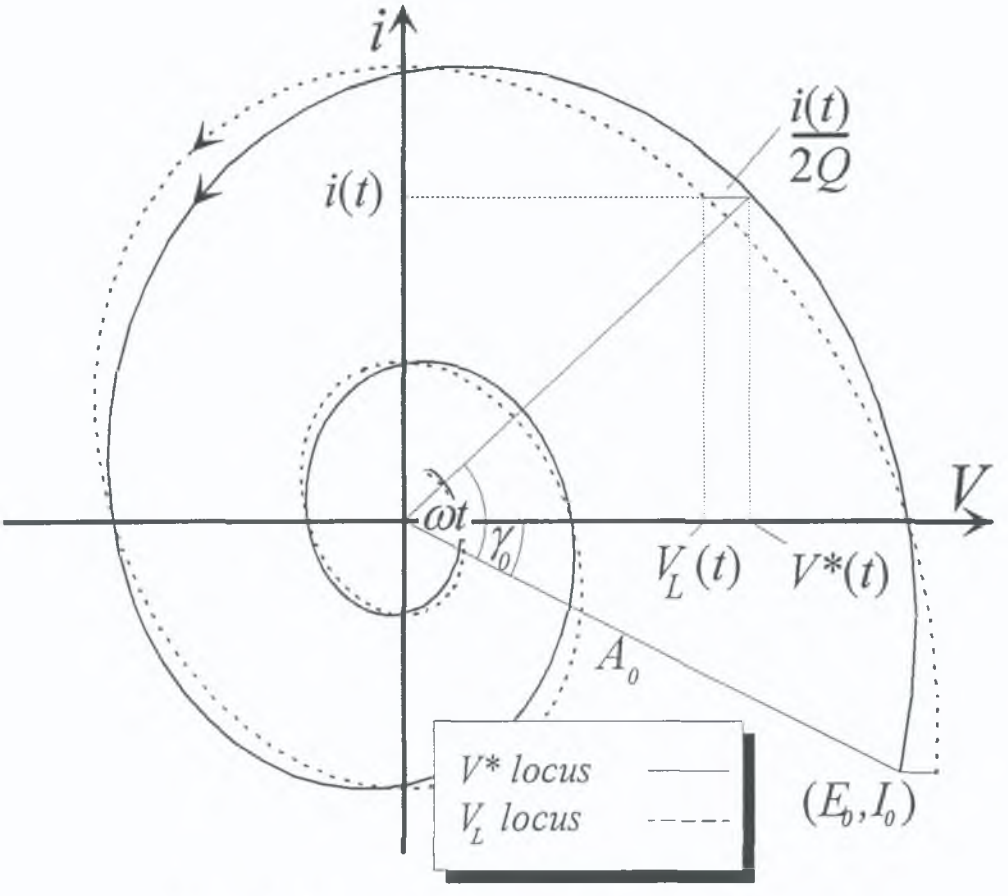

Figure 3.3: Loci of V_L and V^* for free oscillations.

The logarithmic spiral described by the V^* locus, will become an important aspect of this presentation allowing the establishment of the steady-state cycle of the SRC and an approach to a better understanding of its operation. The case of the other spiral, the V^{**} locus is treated in appendix A.

3.3. Forced oscillations

Consider the circuit shown in Fig. 3.4. The switch S alternates between two positions causing voltage steps at the input of the RLC circuit. The frequency and duty cycle of the switching will influence the resultant wave forms in the circuit.

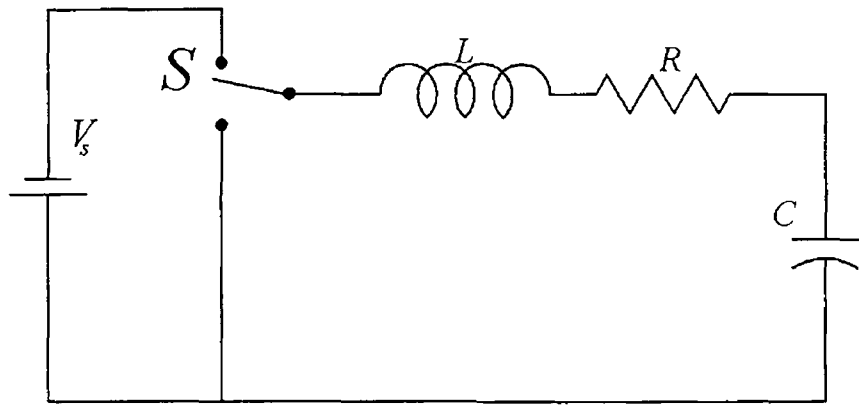

Figure 3 4 Series *RLC* combination with excitation

Fig 3 5 represents the loci of V^* and V_L in the state plane Consider V^* since V_L can be derived from it It rotates from an initial position defined by $A_0 \& \gamma_0$, through an angle of ωT such that

$$T = \frac{1}{2f}$$

to a point $U\ (E_T, I_T)$ At this point, the input voltage switches to zero This voltage step is directly subtracted from V_L and V^*, since the continuity of the current must be respected

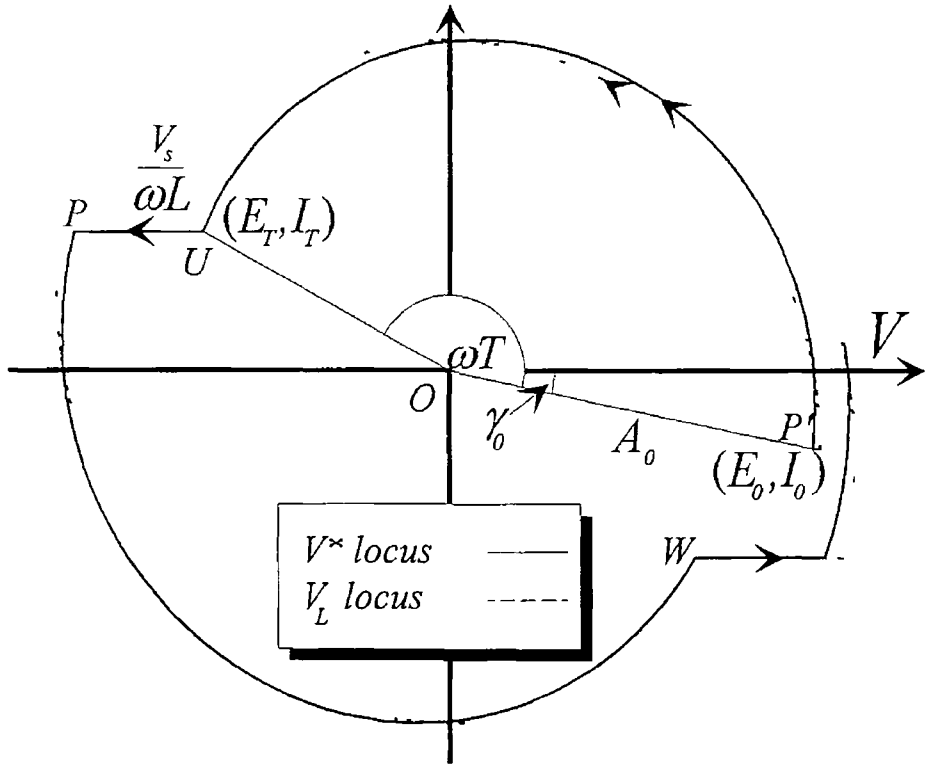

Figure 3 5 Loci of V_L and V^* with a square-wave driving voltage

The result is a horizontal discontinuity of magnitude $\frac{V_s}{\omega L}$ in both loci (Fig 3 5) to arrive at the point P From P, the locus will continue as shown to a point W, where another switching of the input voltage takes place The locus will converge on a steady-state or limit cycle which is characteristic of the steady-state operation of the converter

3 3 1. Limit cycle

For a duty cycle of 50%, which is our case, the limit cycle will be symmetrical in the origin At a switching frequency, f_S, above the resonant frequency, f, which is defined by

$$f = \frac{1}{2\pi}\sqrt{\left(\frac{1}{LC}\right) - \left(\frac{R}{2L}\right)^2} \qquad (3\ 10)$$

the circuit will operate in CCM 1 CCM 2 operation will be discussed later It is useful to be able to find the limit cycle directly The condition for this cycle is that the point P be symmetrical in the origin to the point P' For this to be the case, we must have

$$I_0 = -I_T \qquad (3\ 11)$$

$$E_0 = -(E_T - \frac{V_s}{\omega L}) \qquad (3\ 12)$$

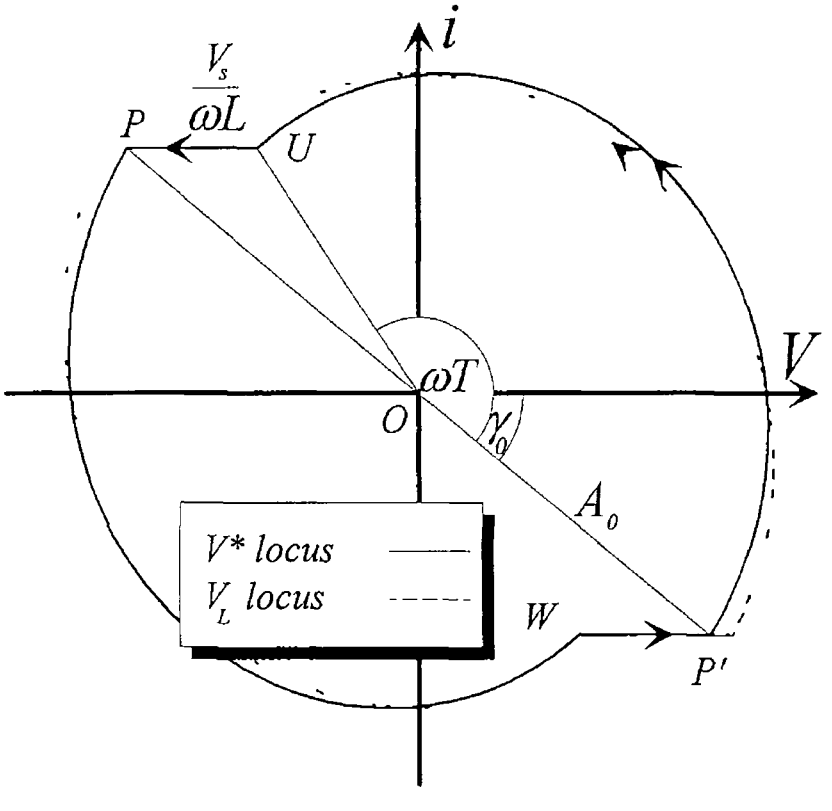

Figure 3 6 Limit cycle of V_L and V^* loci

The result will be a closed trajectory (Fig 3 6) with two horizontal discontinuities which correspond to V_s switching off (U) and on (W)

3 4 Construction

The properties of the spiral described by the V^* locus in the state plane combined with the obligation for symmetry in the steady-state cycle can be exploited in order to construct the limit cycle of the SRC for given load and control conditions This can be done for the two modes of operation found in the literature, CCM 1 and 2 Each mode of operation has two possible control schemes and the technique presented works with both

A similar construction can be carried out for V^{**} (the spiral associated with v_C), but it is found to be less interesting because of its complexity and the fact that once the steady-state of V^* found, the other wave forms can be derived from it As an indication of the complexity of the construction, the CCM 1 - T and T_C control cases for construction of V^{**} are carried out in appendix A

3 5 CCM 1 construction

The two control schemes involved in this case are

- CCM 1 - T control the independent variable used to control the converter is the frequency, thus giving a well defined periodic time, $2T$
- CCM 1 - T_C control control through transistor conduction time, T_C

3 5 1 CCM 1 - T control

This is the simplest case of construction and is achieved as follows (refer to fig 3 7)

- Draw a horizontal line PP'
- Bisect this line to situate the point O
- The magnitude OP' is considered as unity
- Construct the line OU' at an angle ωT to PP'
- Situate the point U on the line OU', in such a manner that $|OU| = e^{-\alpha T}$
- Construct the line UP This line corresponds to the switching of the supply voltage V_s So the magnitude of the initial condition A is given by
  $A = \frac{V_s}{\omega L}\left|\frac{OP'}{UP}\right|$
- The magnitude of the angle γ can be read directly off the diagram once the position of the voltage axis is known The voltage axis is parallel to UP and goes through the origin

For completeness the locus in Fig 3 7 has been closed, but it is obvious that it is symmetric in the origin and that the construction of the line UP is sufficient to ensure a valid limit cycle

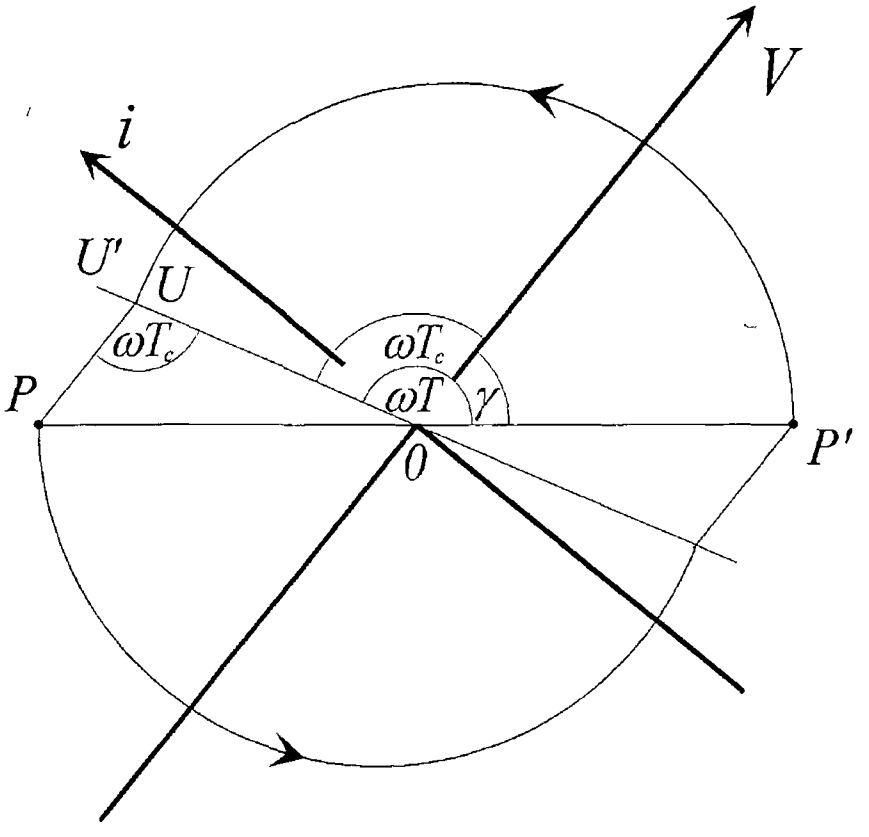

Figure 3 7 Construction of limit cycle knowing the periodic time, T

The case of T control does have a general analytical solution that applies to CCM 1 and 2, but this solution gives little insight into the operation of the SRC The analysis in question is given in Appendix B for reference

3 5 2 CCM 1 - T_C control

This case can not be solved analytically due to the fact that the diode conduction time is not known, and finding it involves the solution of transcendental expressions A graphical solution is possible based on the construction of Fig 3 7 It is clear that the conduction angle of the transistors is $\omega T - \gamma$, or the angle that OU makes with the V-axis This angle can also be found at PUO, since PU is parallel to the V-axis So in order to find the limit cycle for a given T_C, it is sufficient to construct the locus of U such that the angle PUO be equal to ωT_c, and find it's intersection with the spiral given by the load in question This can be done as follows (refer to Fig 3 8)

- Commence as before with PP' and the point O
- The half-spiral for the load in question is drawn
- Construct a right-angled triangle PRS such that $|PR| = \frac{|PO|}{2}$ and

$\angle PSR = \omega T_c$

- Now a circle of radius $|SP|$, centred at S, will cut the spiral at a point, U, such that $\angle PUO = \omega T_c$
- As before the V-axis is parallel to PU and the i-axis is at right-angles to it

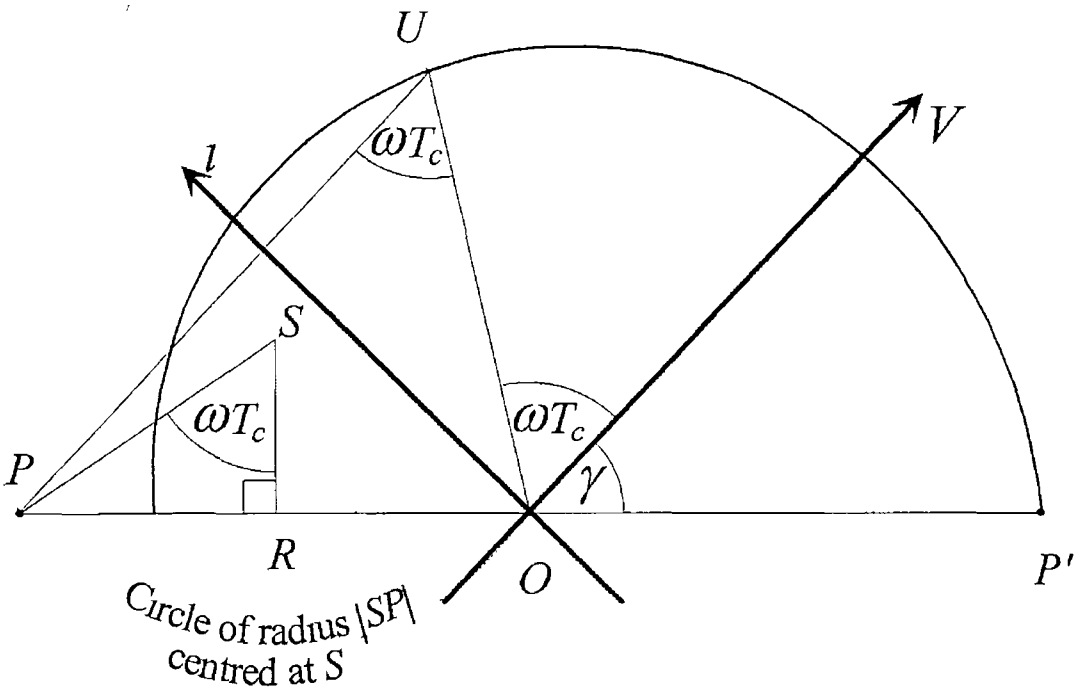

Figure 3 8 Locus construction knowing the transistor conduction time, T_c

3 6 CCM 2 construction

In this case, $\frac{1}{2} < \frac{f_s}{f} < 1$ To approach the limit cycle that respects this condition, let us consider the border-line case between CCM 1 and 2, i e $\frac{f_s}{f} = 1$ It is seen by comparing Fig 3 9 and Fig 3 6 that the diode conduction angle goes to zero and that the switching takes place at zero current

Now the logical progression in the case of ever increasing conduction angle, would seem to be a diode conduction angle that increases as well This gives rise to the limit cycle shown in fig 3 10 The conduction angle of each switch is greater than π

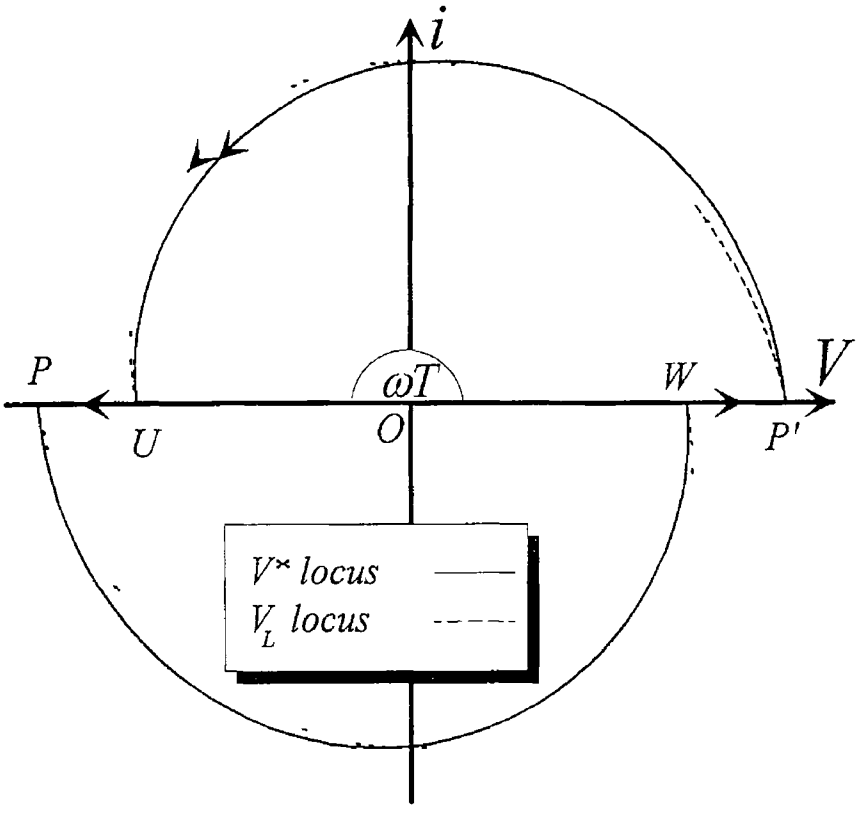

Figure 3 9 V_L and V^* loci at resonance

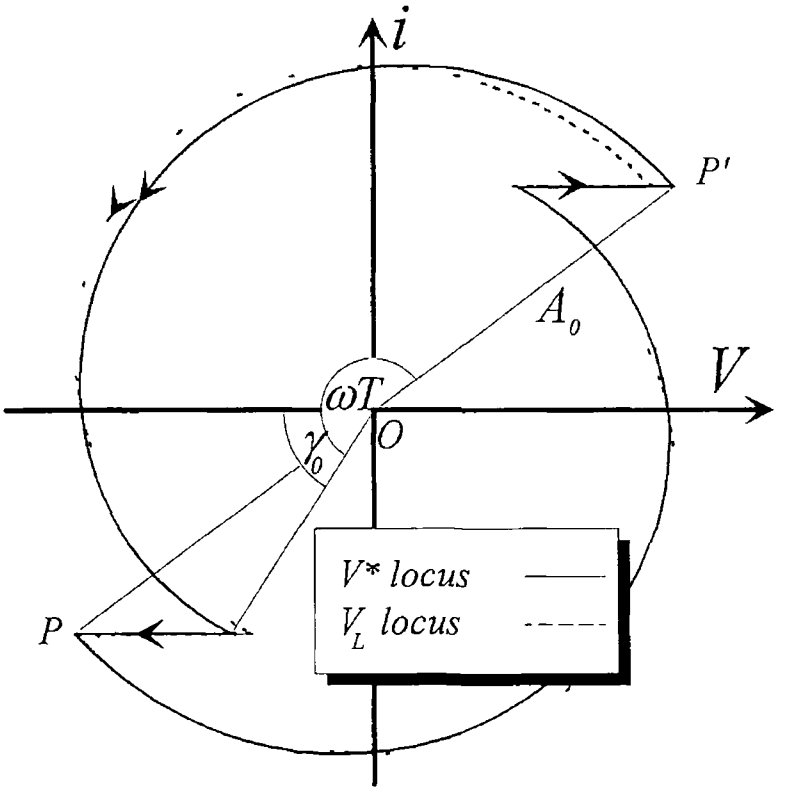

Figure 3 10 Limit cycle in CCM 2 mode

As before, the steady-state operation for each of these cases can be found in a similar manner to the previous cases The two control schemes involved are

- CCM 2 - T control frequency control
- CCM 2 - T_D control diode conduction time, T_D, control

3 6 1 CCM 2 - T control

The construction for this case is carried out in exactly the same manner as for CCM 1 The result is only slightly different (refer to Fig 3 11)

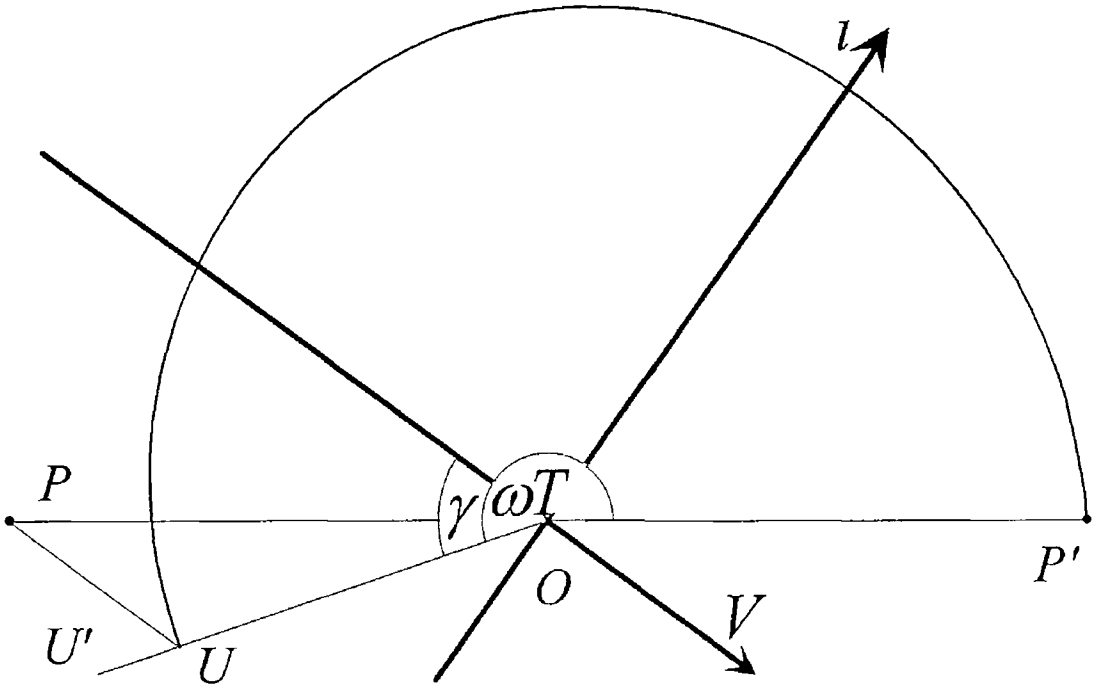

Figure 3 11 Construction of locus knowing periodic time, T

3 6 2 CCM 2 - T_D control

This construction is based on the fact that from Fig 3 11

$$\angle PUO = \pi - \gamma$$

Where $\gamma = \omega T_D$

and that a given $\angle PUO$ can be constructed in a similar manner to ωT_C in CCM 2 (refer to Fig 3 12) The difference in this case is that the spiral arc is continued through an angle of 2π The intersection of this arc and the arc of a circle is always below the line PP'

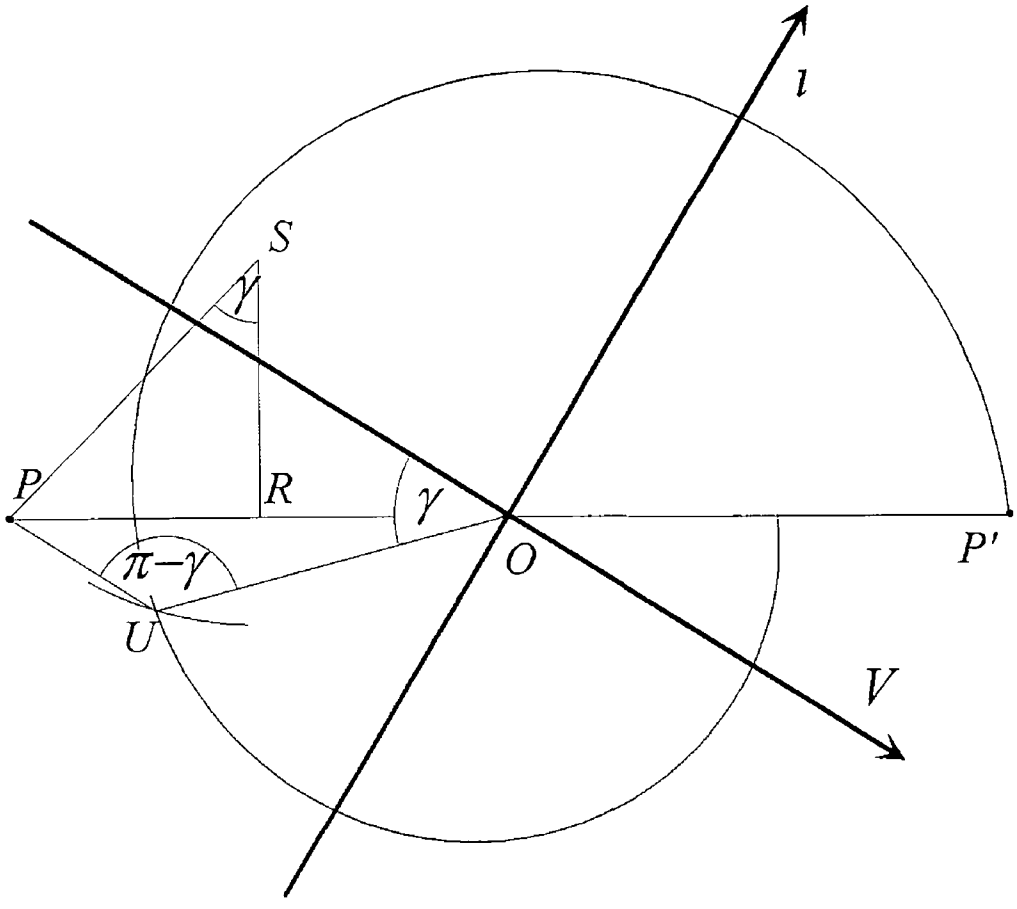

Figure 3 12 Locus construction knowing diode conduction time, T_D

4. GENERAL OBSERVATIONS ON SRC THROUGH STATE PLANE

4.1. Introduction

The state plane technique is not limited to quantitative analyses such as finding the initial conditions that give the limit cycle for specific load and frequency conditions as shown in chapter 3.. It is just as well adapted to carrying out qualitative analyses such as comparison of two control schemes and can be used to demonstrate certain properties of the SRC. With practice, the technique allows general appreciations to be carried out directly on a construction graph of the type shown in Fig. 3.8. It also allows more complex specific analyses, supplying the information necessary for the construction of a case or series of cases in the state plane or the initial conditions necessary for the calculation of peak current or voltage or switching current. Certain phase or relative amplitude observations can be made without needing to calculate the non-normalised values.

4.2. Time domain representation

In order to demonstrate the contrast between the state plane representation and the more traditional time domain representation, three limit cycles are constructed for the same load at different frequencies (Fig. 4.1(a)). The initial conditions for each case are read off the construction graph and used to produce the v^* loci in the state plane (Fig. 4.1(b)) where the relative scales of each locus are respected. The smallest and largest conduction angles represented are only theoretical, they are not encountered because of practical limitations. However, by observing them, it is possible to get an idea of the vast range of power variation possible with this circuit structure through switching frequency variation. The power in the resistive part of the load is proportional to i_{rms}^2. As a first approximation, i_{rms} is proportional to peak current, I_{peak}. In Fig. 4.1(b), it is clear that I_{peak} varies by a ratio of 5.5 giving roughly a power variation ratio of over 30. In reality, the practical constraints limit this variation to 10, but this demonstration using the state plane shows the theoretical possibilities of the series resonant structure.
The time domain wave forms corresponding to the three cases above are shown in Fig. 4.2. In [38], Kazimierczuk et al summarise the state plane as follows "The state plane provides a compression of information which allows the designer to uniquely examine the non-linear dynamics of resonant converter operation". A comparison of Fig. 4.1(b) and Fig. 4.2 demonstrates this compression.

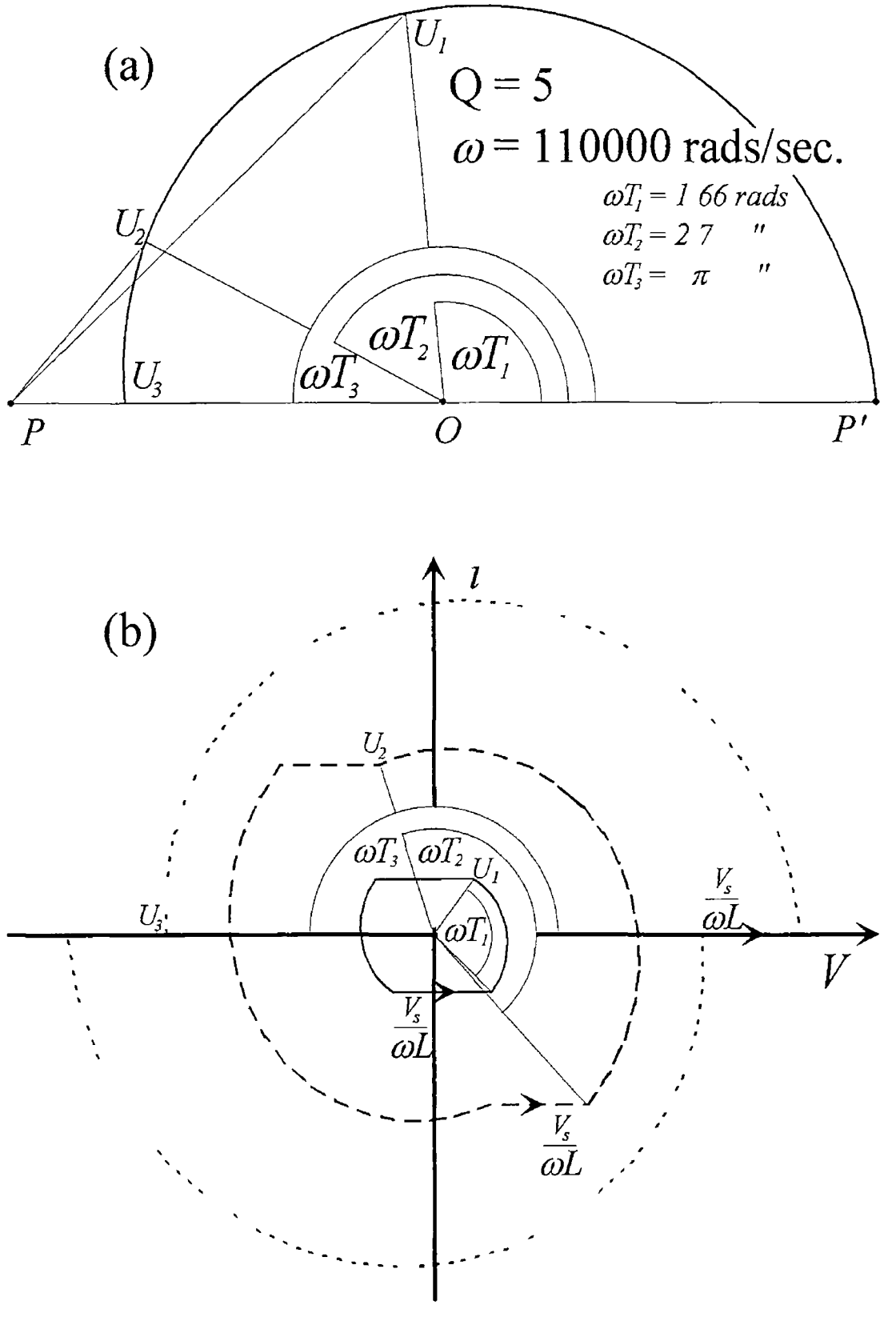

Figure 4 1 (a)Construction of limit cycles for the same load at three different frequencies and (b) display of the same limit cycles in the state plane with the correct proportions restored

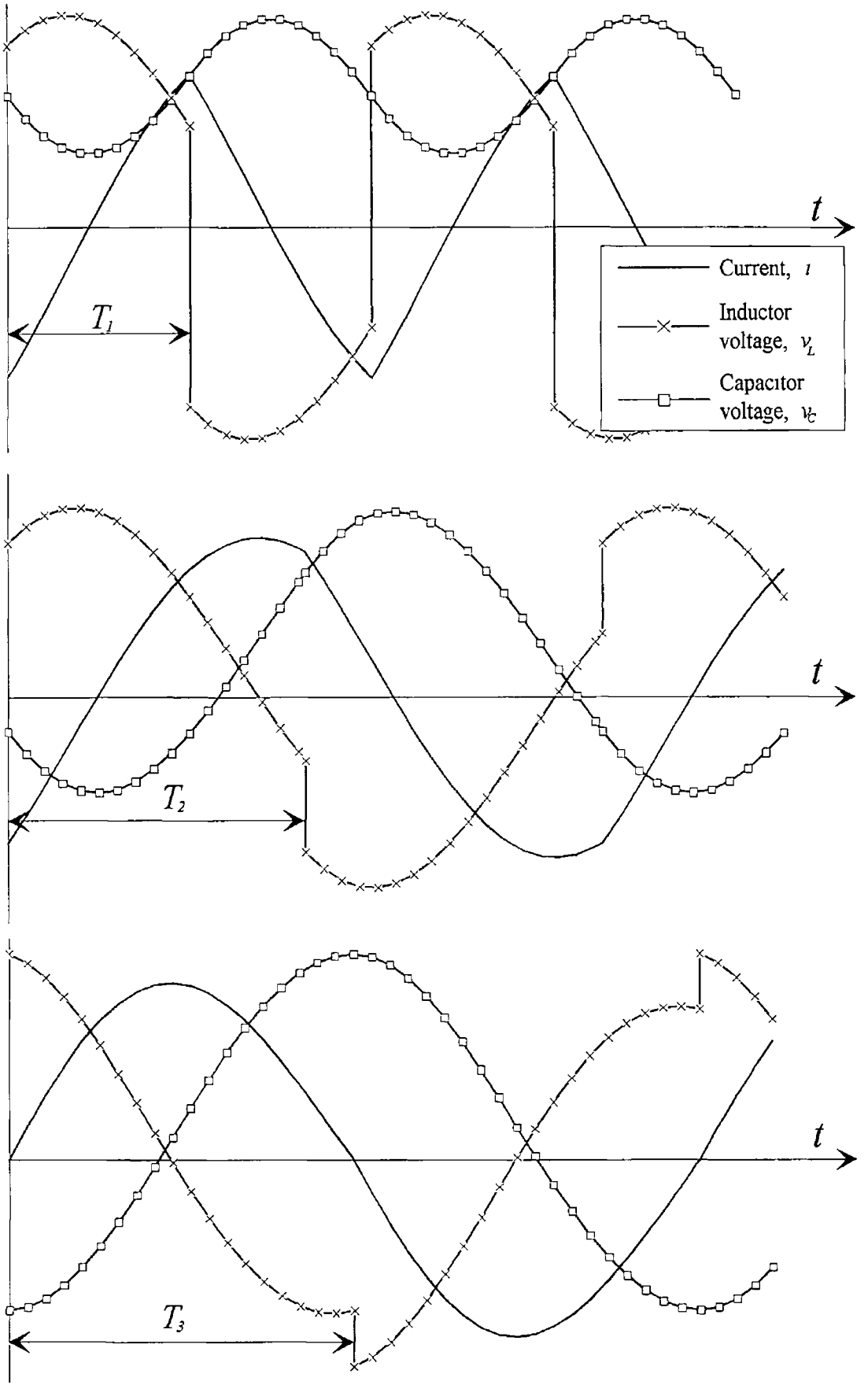

Figure 4 2 Time domain wave forms for a given load at three different working frequencies

4 3 Comparison of T and T_C control

The basis of the graph in Fig 4 3 can be found in equation (3 2) Rewriting with respect to OP' gives

$$\vec{S}' = e^{-\frac{\theta}{2Q}} e^{-j\theta} \qquad (4\ 1)$$

Where $|\vec{S}'| = \frac{|\vec{S}|}{A}$

$\theta = \omega t$

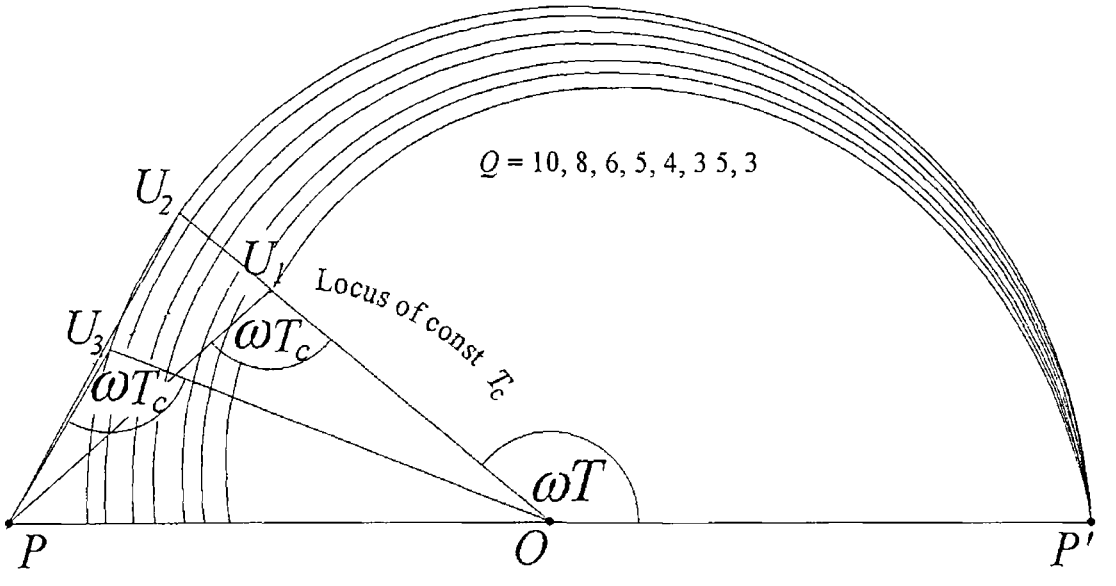

Figure 4 3 Comparison of load change for T and T_C control

With this form of the spiral equations, it is possible to draw the spiral normalised with respect to OP' for given values of Q and carry out comparisons of various working points For example, it is interesting to compare the modification of the circuits working point due to a change in load conditions This can be done for the case of each of the different control approaches In Fig 4 3, a diagram has been prepared with a family of spirals for varying Q-factors in such a manner as to allow the construction of CCM 1 stable cycles Consider a point U_1 on the innermost spiral such that U_1P is the supply voltage, $\frac{V_s}{\omega L}$, giving a stable cycle This stable cycle can be produced

- by directly controlling the frequency at f, such that $T = \frac{1}{2f}$
- by controlling the transistor conduction time at T_C

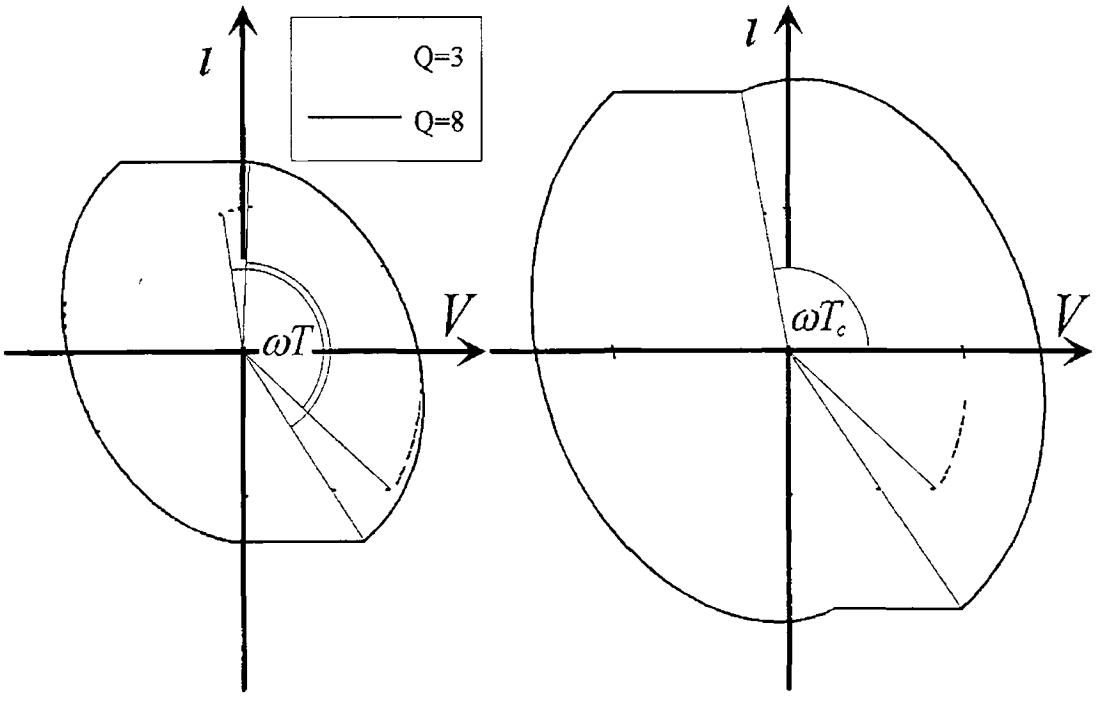

Figure 4 4 Comparison of load change for constant (a) frequency and (b) transistor conduction time, T_C

Now the result of a variation in Q-factor for a constant control parameter can be observed in each case In the first case, the constant frequency locus is a straight line OU_2 At the working point U_2, the scale of the diagram (defined by $|U_2P|$) has changed little compared to U_1

The voltage axis (not shown to avoid confusion), which is parallel to U_2P, has moved indicating a variation of the duty cycle between transistor and diode In comparison, the locus of constant T_C is the arc of a circle U_1U_3 In this case we see that the scale of the diagram has drastically increased since $|U_1P| \approx 2|U_3P|$ The voltage axis has assumed a position similar to the case U_2, but the variation is in diode conduction time, since T_C is constant It is obvious that a similar observation can also be made when comparing the different control schemes possible for CCM 2 operation The consequences of this difference are more striking when the diagram is redrawn with the relevant scaling corrections The constant frequency case can be seen in Fig 4 4(a), and the constant transistor conduction time in Figure 4 4(b)

4 4 Max diode and transistor conduction time

It is interesting to observe the diode conduction angle in the case of CCM 1 operation and the transistor conduction angle in the case of CCM 2 operation As can be seen from Fig 4 5, in the case of CCM 1 operation, for a given diode conduction angle, γ, two possible periodic times exist, T_1 and T_2 It can also be seen that the case of the

tangent PU to the spiral gives the maximum possible diode conduction angle OPU for the load in question, and a single possible conduction time

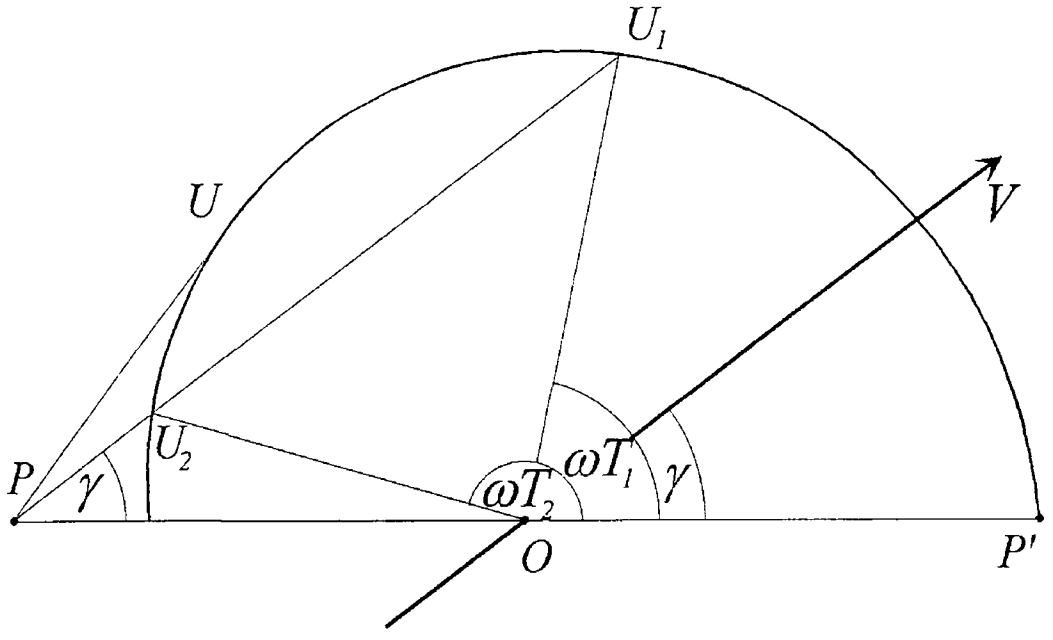

Figure 4 5 Observation of diode conduction angle in CCM 1 mode

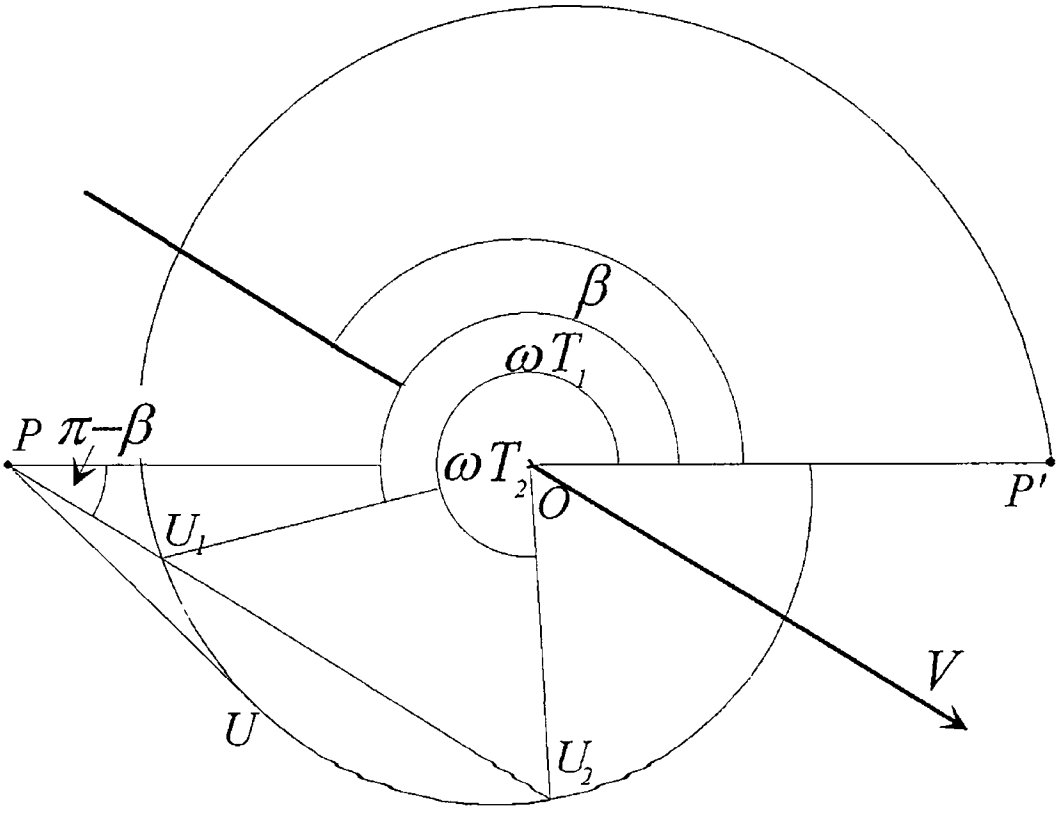

Figure 4 6 Observation of transistor conduction angle in CCM 2 mode

A similar phenomenon is observed for the transistor conduction angle in the case of CCM 2 operation (see Fig 4 6) In this case, there exists a minimum conduction angle for a given load

4 5 Capacitive switching-aid network

When operating in CCM 1 the basic SRC circuit can be modified to reduce transistor switching losses by adding a capacitor in parallel with each transistor as described in section 2 2 3 These capacitors are called upon during the switching transitions in order to slow the rise of the collector-emitter voltage across the transistor that has switched off Their value is defined by the required slope of the voltage transition in worst case conditions (i e max switched current) An order of magnitude is one-tenth of the resonant capacitor value The transition times in question are short compared to the switching period but it is interesting to study them because they give rise to very characteristic behaviour of the SRC which imposes limits on its operating frequency The observation of the behaviour of the SRC during these transitions is possible in the state plane In order to carry out this analysis, it is necessary to develop a technique for finding the limit-cycle when the position of the axes is known as opposed to the techniques discussed up to now which define the position of the axes once the limit cycle is found

4 5 1 Steady-state with fixed axes

This technique stems from observations on Fig 3 7 The expression for the two arcs of spirals described in this diagram take P and P' as starting points

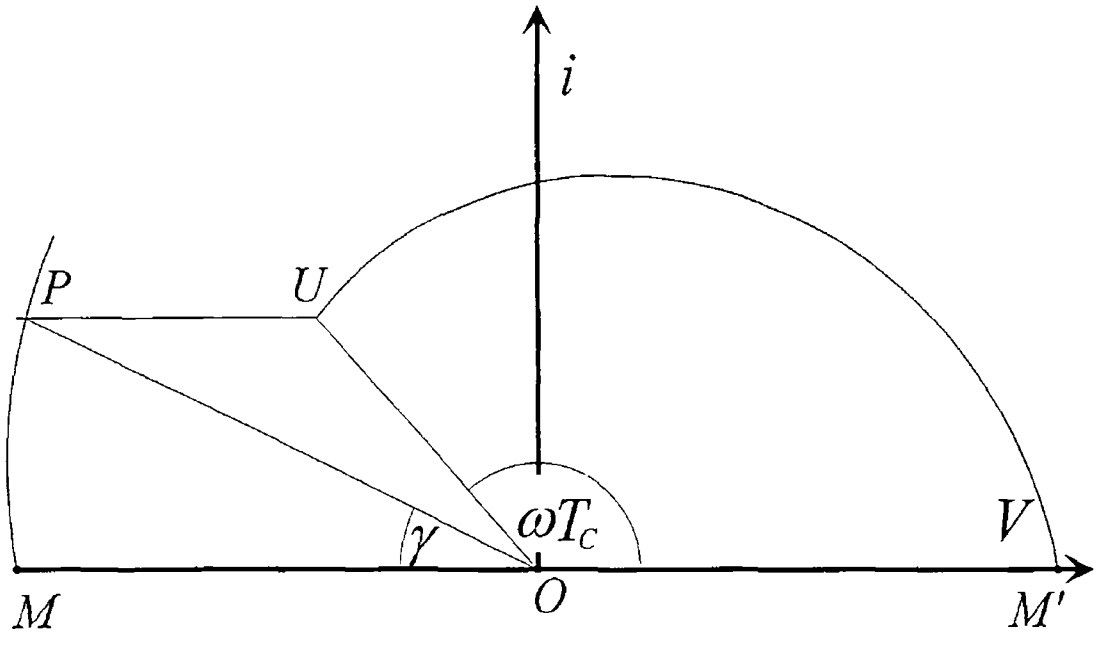

Figure 4 7 Construction of limit cycle knowing position of axes

It is possible to arrive at the same result taking the v-axis intersects as the starting points of the construction as follows (see Fig 4 7)

- Draw a line MM' Position O at the bisection of this line
- From M', construct a decaying spiral centred at O, $e^{-\frac{\theta}{2Q}}$, through an angle, ωT_C, to a point, U
- From U, draw a horizontal line as in the diagram
- From M, construct a growing spiral centred at O, $e^{\frac{\theta}{2Q}}$, to intersect with the previous line at P
- As usual, the length of UP defines the scale of the diagram

4 5 2 Steady-state with capacitive switching-aid network

The above analysis approach allows the study of the effect of switching-aid capacitors on the circuit because to do so it is necessary to have the axes situated before the limit cycle is constructed

Consider the two equivalent circuits shown in Fig 4 8 Fig 4 8(a) represents the SRC during the conduction of the switches (transistor or diode) that drive it Fig 4 8(b) is the equivalent circuit during the switching transitions when the capacitor C_S is added in series with the resonant capacitor to form a secondary resonant circuit In the phase plane, the circuit will function as usual during the conduction of the transistor because C_S is short-circuited Once the transistor has been switched off, the modification of the circuit gives rise to modifications in the circuit parameters (ω_s, Q_s) This change in ω and Q prevents us from continuing as a spiral in the same plane, because the scaling factor for the horizontal axis is no longer the same In order to continue the trajectory as a spiral, it is necessary to define a new scaling factor for the v-axis, $\omega_s L_s$

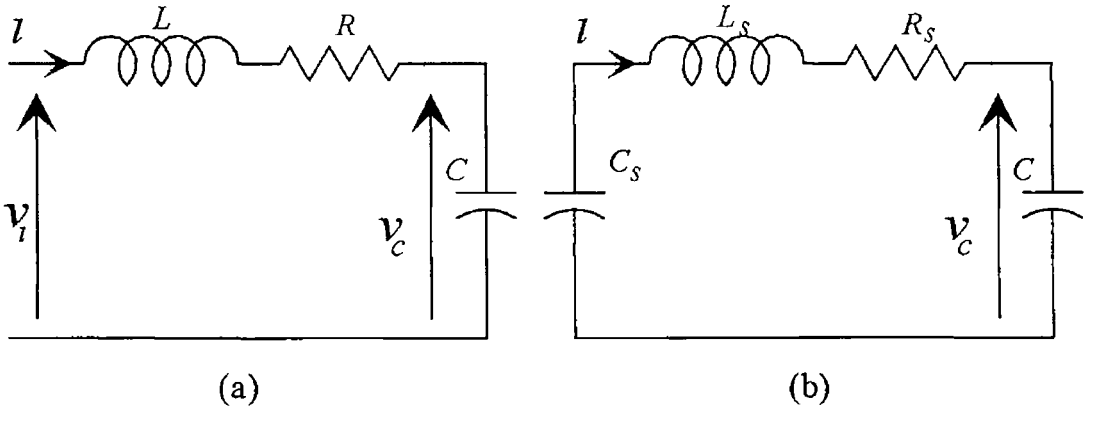

Figure 4 8 Equivalent circuits for induction SRC during the conduction of (a) the switches and (b) the capacitive switching-aid network

For the sake of clarity, the new scaling factor is represented on a separate plane as in Fig. 4.9. Once the spiral drawn, it will be easy to translate it back to the original plane. This operation can be carried out in two sections on the same plane by simply applying the relevant scaling factor to each trajectory. The change in scale applied to the point U defines the starting point of the spiral in this second plane. When the translation back to the first plane is made, the point P can be situated at the intersection of the transition trajectory and the growing log spiral starting from M (Fig. 4.9).

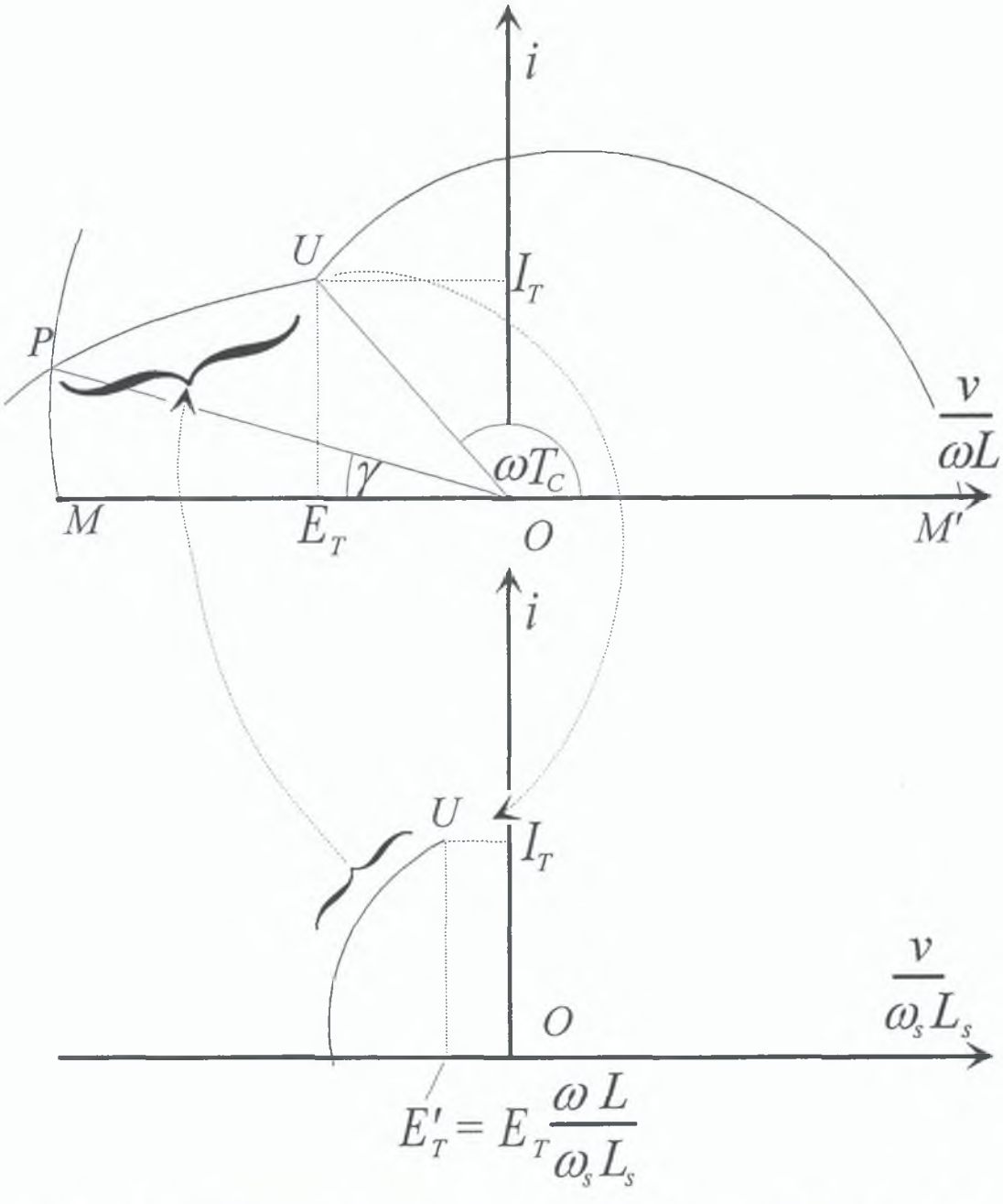

Figure 4.9: Construction of limit cycle with a capacitive switching-aid network.

In order to demonstrate this, it was necessary to know the value of the impedance of the load during the conduction of the switching-aid capacitors. This is modified by the

change in resonant frequency due to a new value of capacitor in the circuit The impedance measurement technique described in chapter 5 is difficult to apply over a period as short as that of the switching transition, because the system of equations is ill-conditioned We can assume that the impedance variation that takes place is entirely due to the change in resonant frequency In this case, in order to extrapolate the values of the modified impedance, the ratio of change of the R and L components due to a similar frequency change was measured on the RLC-bridge

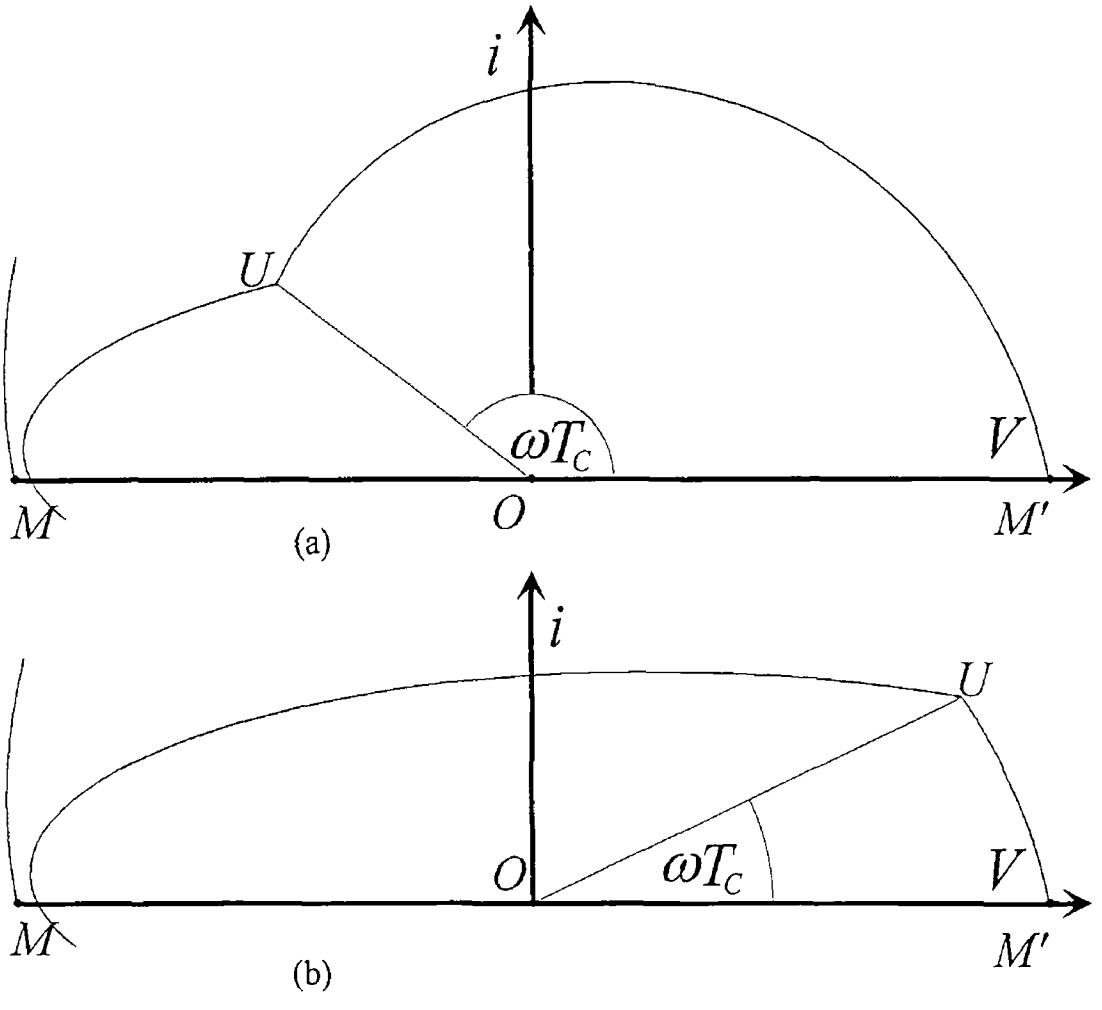

Figure 4 10 Observation of induction SRC behaviour when frequency is (a) too low or (b) too high for a given load

The inclusion of switching-aid capacitors in the SRC circuit imposes a constraint on the frequency range in which it can operate As can be seen from Fig 4 10, too long (a) or too short (b) a transistor conduction time can prevent the transition trajectory from intersecting with the growing spiral as it should in order to ensure a closed trajectory This will result in an undesired end to the SRC's operation in the case where the switches conduction is inhibited if the voltage across it is not zero If the switches can be switched on at non-zero voltages, then the generator will operate in a zone where

switching losses are extremely high due to the discharge of C_S being completed through the transistor which has been switched on This is an undesirable state of operation for the transistors who's ratings and ventilation have been defined for losses which do not include the above-mentioned

5 LOAD MEASUREMENT IN INDUCTION HEATING APPLICATIONS

5 1 Introduction

This chapter deals with the problem of measuring the load of an induction heating generator The previous chapters have exposed techniques for the analysis of the SRC used in the induction application These techniques are all based on a good knowledge of the load impedance of the converter The nature and variety of this load has been discussed in section 1 2 Section 1 5 exposes the difficulties encountered in modelling a given case of loading These two sections combined lead to the conclusion that there is little hope of developing a global model for the load In the light of this fact, it is necessary to have a valid load measurement technique, in order to confirm the validity of techniques such as presented in the previous chapters This measurement technique can also be used to establish the zone of impedance in which the generator will operate and to study the effects of various utensil materials, sizes, and positions relative to the inductor It will also serve to check the results of load modelling exercises and in this way contribute to perfecting their algorithms The existing measurement techniques have pitfalls that have been discussed in section 1 5 , which leads to a proposition of a new measurement method A direct measurement of the load parameters while it is working in-circuit, and an analysis of these parameters must yield a representative result A technique is presented whereby a numerical analysis is carried out on the circuit wave forms in order to extract the equivalent circuit values In order to keep this technique as general as possible, the parameters that are measured are the voltage across the load and the current flowing in it In this way, abstraction is made of the generator circuit

5 2 Analysis

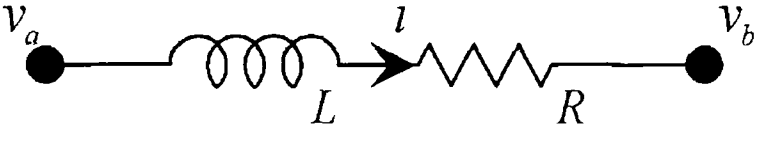

Figure 5 1 Load equivalent circuit

From section1.1. the circuit in Fig 5.1 represents the load of an induction generator. Assuming L and R constant, which has been proven acceptable, we can write the following equation:

$$v_a - iR - L\frac{di}{dt} = v_b \tag{5.1}$$

Using a backward difference discretization method [39], this can be rewritten

$$(v_a - v_b)_k \Delta t = i_k R\Delta t + L(i_k - i_{k-1}) + \varepsilon_k \tag{5.2}$$

where

ε = error term.
x_k = observed value of the variable x, at a given instant.
x_{k-1} = observed value of the variable x, at a time, Δt, before.

With n+1 observed values of these variables as regressors and R and L as unknowns, a least squares formulation can be written as follows:

$$Y = HX + E \tag{5.3}$$

where

$$Y = \begin{pmatrix} (v_a - v_b)_1 \Delta t \\ \cdot \\ \cdot \\ \cdot \\ (v_a - v_b)_n \Delta t \end{pmatrix} \qquad H = \begin{pmatrix} i_1 \Delta t & (i_1 - i_0) \\ \cdot & \cdot \\ \cdot & \cdot \\ \cdot & \cdot \\ i_n \Delta t & (i_n - i_{n-1}) \end{pmatrix} \qquad E = \begin{pmatrix} \varepsilon_1 \\ \cdot \\ \cdot \\ \cdot \\ \varepsilon_n \end{pmatrix}$$

$$X = \begin{pmatrix} R \\ L \end{pmatrix}$$

Following sets of measurements of v_k and i_k, the above overdetermined may be solved (in a least squares sense) for R and L (X) [40]:

$$X = (H^T H)^{-1} H^T Y \tag{5.4}$$

5.3. Measurement, filtering and verification

The measured wave forms were found to be noisy. Power density FFT's of the signals showed the noise to be coloured as seen in the example of Fig. 5.2. In order to filter this noise two FIR digital filters were used.

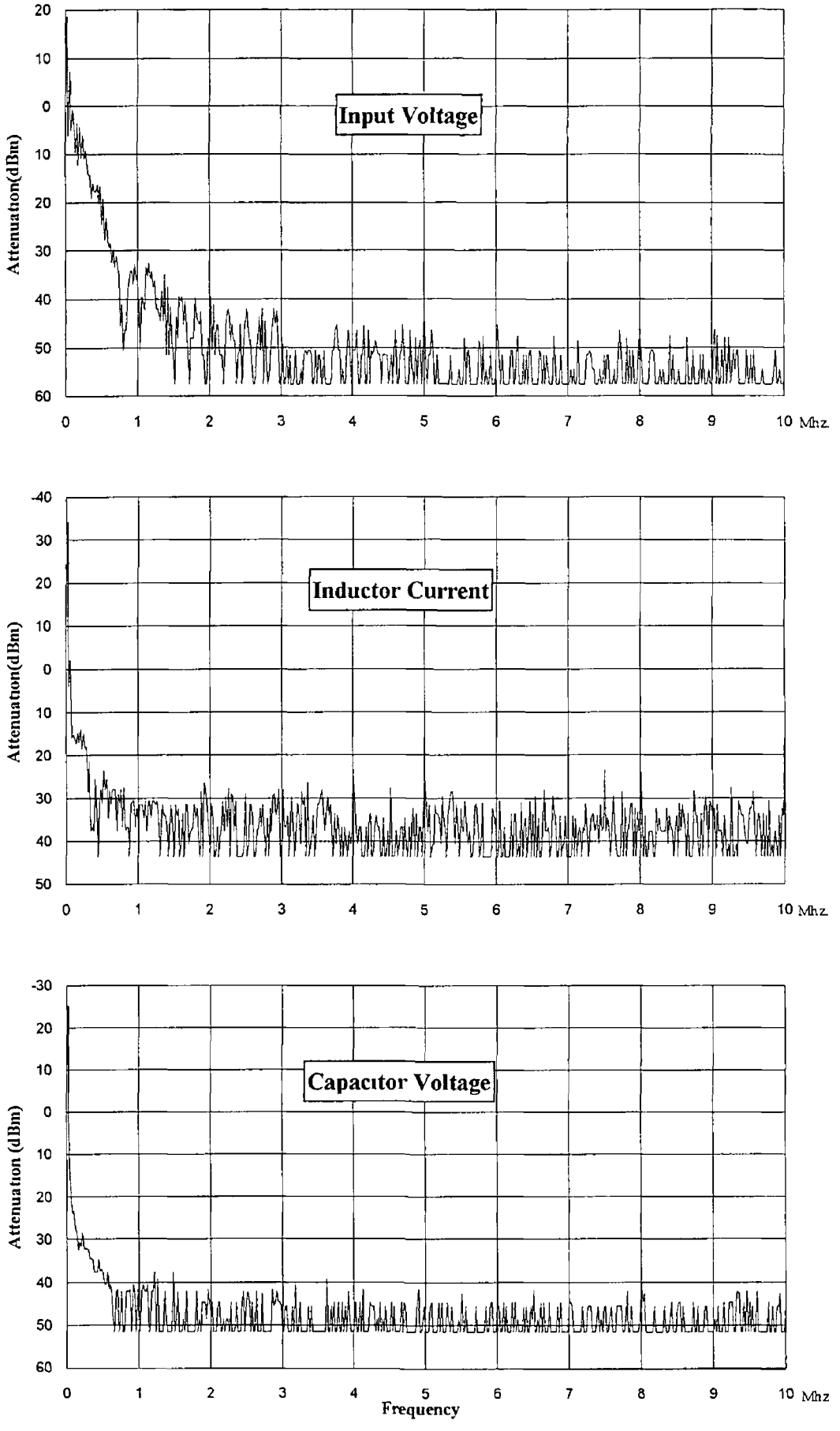

Figure 5 2 Power Density FFT's of measured wave forms before filtering

Two separate filters were needed due to the difference in signal bandwidth between the current and the capacitor voltage on one side and the input voltage on the other This difference was to be expected since the former are semi-sinusoidal signals while the latter is a square-wave The filter characteristics are given in Fig 5 3 The lower 3 dB frequency is 800 khz and is applied to the capacitor voltage and the current The upper is 2 9 MHz The results of the filtering on the respective wave forms can be seen in Fig 5 4

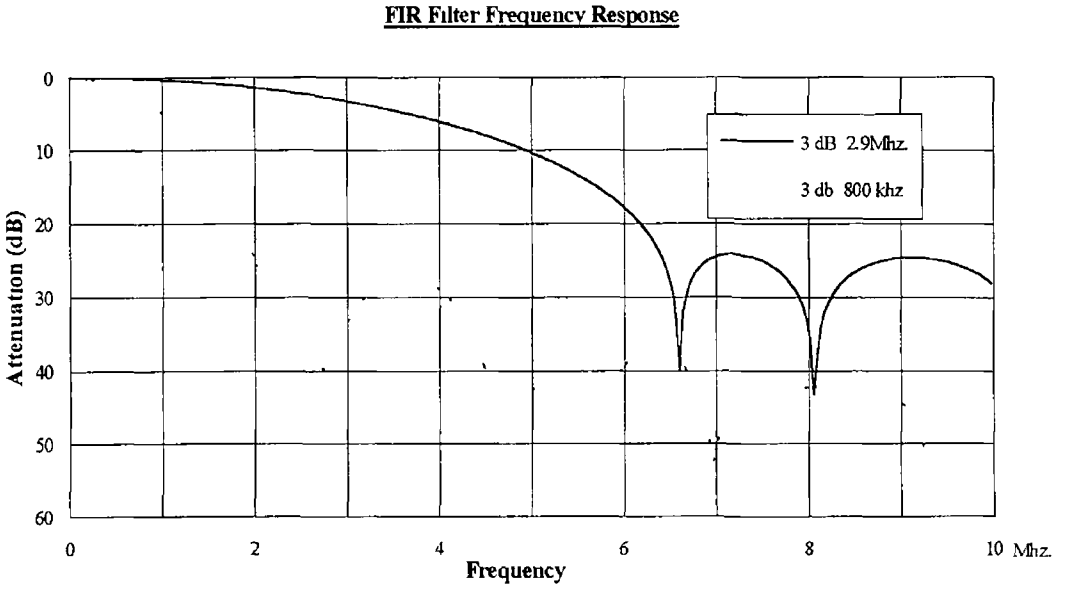

Figure 5 3 FIR Filter frequency response

The measurements were made over at least one generator cycle with a digital storage oscilloscope and the measured data transferred to a PC for analysis A short programme carries out the matrix operation Data during the switching transitions is discarded because the switching-aid capacitors alter the circuit impedance

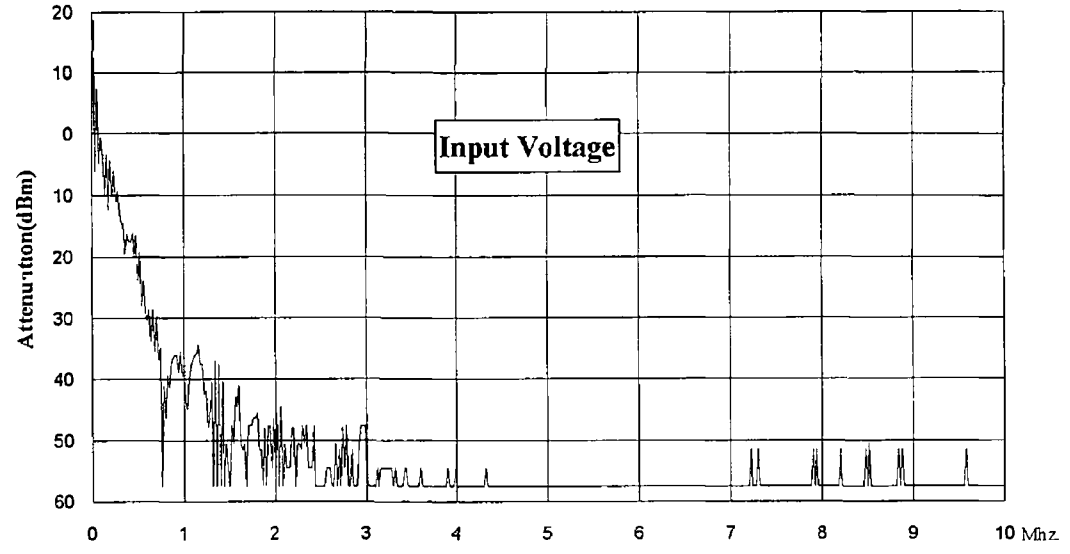

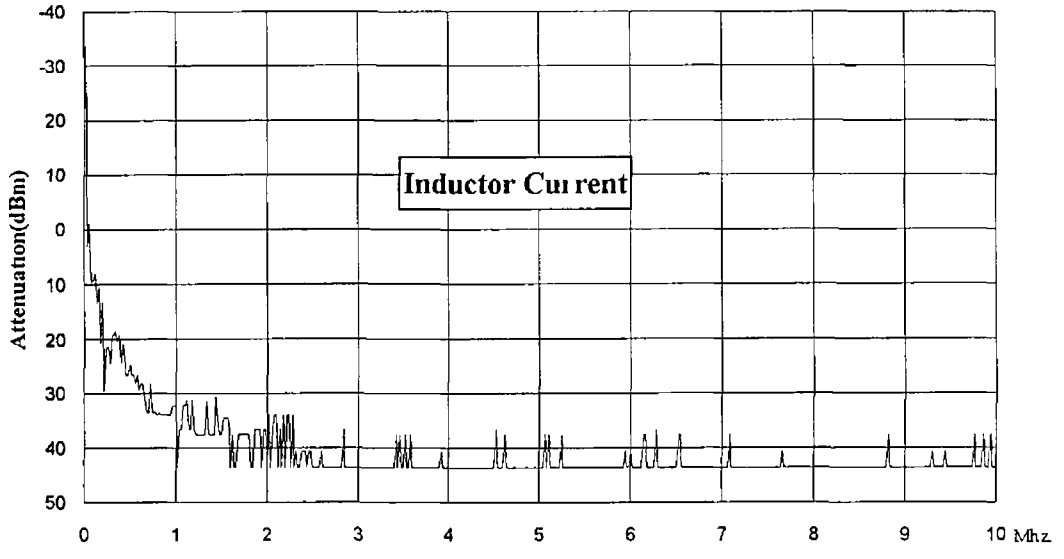

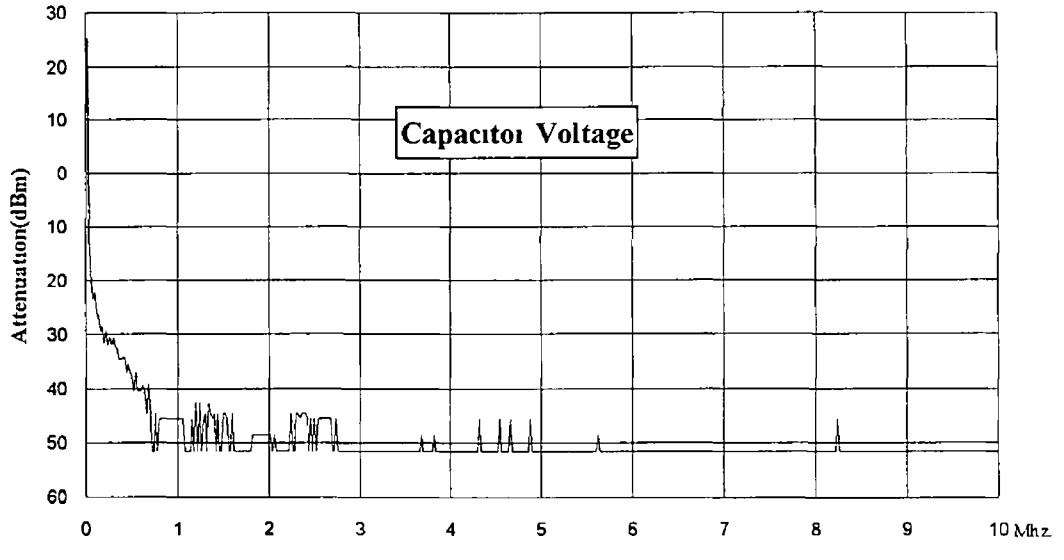

Figure 5 4 Power Density FFT's of measured wave forms after filtering

With a good knowledge of the power consumed at the source, the efficiency, and the current in the load, the R component of the result can be verified using the relationships:

$$P_L = I_{rms}^2 . R \tag{5.5}$$

$$P_C = \frac{P_L}{\eta} \tag{5.6}$$

where

P_C = mains power consumed by the generator.
P_L = power in load.
η = efficiency.
I_{rms} = r.m.s. load current.
R = resistive component of the load.

It is necessary to run a simulation of the complete generator circuit to verify the accuracy of the L value.

5.4. Results

Measurements were made using the professional inductor described in section 2.6. and a resonant capacitor of 470 nF.. Table 5.1 below comprises R and L values for given utensils centred on the same inductor. For each utensil, RLC-bridge values and values yielded by the least-squares analysis described have been measured.

Table 5.1: Comparison of power calculated using measured values of R.

			LEAST-SQUARES			RLC-BRIDGE		
	P_C*	I_{rms} (A)	R(Ω)	L(μH)	P_L/η*	R(Ω)	L(μH)	P_L/η*
U1	6	26.5	7.82	190	5.9	4.5	170	3.44
U2	6	27.2	7.43	185	5.9	5.44	159	4.3
U3	6	27.3	7.55	185	6.05	5.47	157	4.4
U4	4.5	24.9	6.39	133	4.26	3.73	134	2.47
U5	4.5	25.4	6.58	181	4.56	3.05	156	2.15

* Power in kW.

Measurements of power consumed, P_C, and r.m.s. current, I_{rms}, have been made and P_L/η (5) is given in each case knowing that efficiency, η, is around 0.93. We can see that the least-squares values are strikingly closer to reality than the RLC-bridge values.

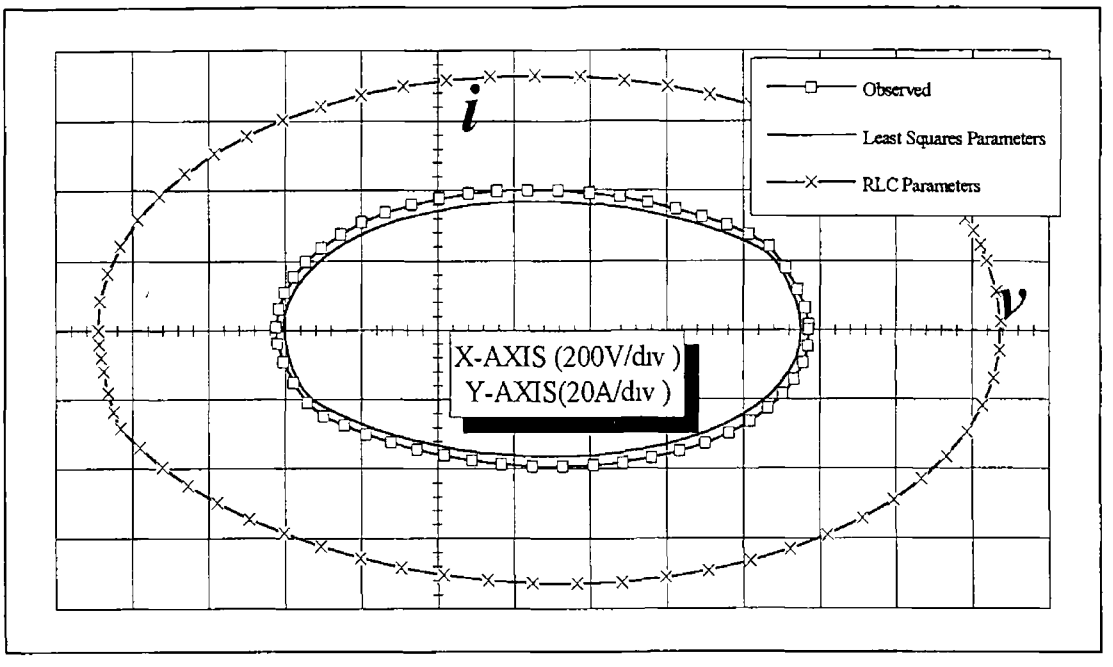

Figure 5 5 Comparison of simulations and measured wave forms at full power for utensil U2

A simulation using the technique described in Chapter 3 allows us to compare the generators cycle at full power for the parameters of utensil U2 measured by the two techniques (Fig 5 5) We can see that the trajectory of the least-squares parameters is much closer to the measured values This confirms the results of table 5 1

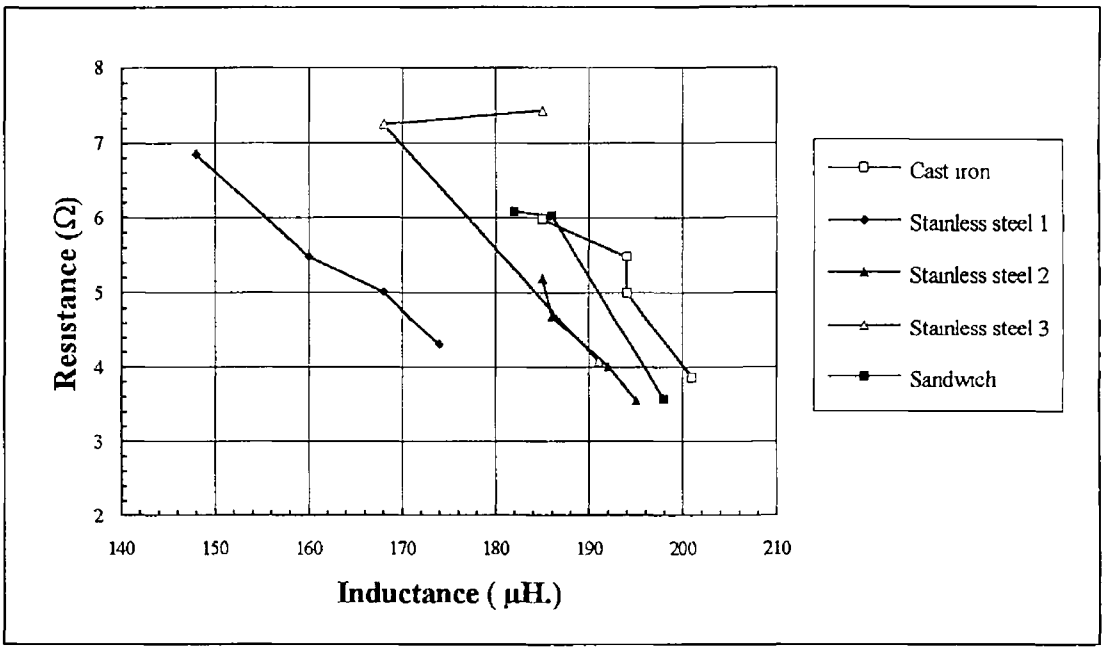

Figure 5 6 Graphical representation of impedance values for various load materials and sizes

A series of measurements were made on a selection of seventeen utensils of different materials and diameters The position with respect to the inductor was central

Although not exhaustive for practical reasons, these can be considered as a good cross-section of available cookware, and give a valid indication of the variety of loads that can be encountered by an induction generator The results of these measurements can be seen in Fig 5 6 where they are represented in the L/R-plane

The points representing utensils made of the same material are joined Five different materials are involved, cast iron, three alloys of stainless steel, a "sandwich" combination of stainless steel and aluminium The results are listed in Table 5 2 A tendency would seem to be that resistance rises and inductance falls as diameter increases The exception to this is the third alloy of stainless steel whose biggest utensil has a higher inductance than the second biggest This could be explained by the fact that the diameter of this utensil is greater than that of the inductor In this case marginal effects might be what prevent a valid extrapolation

Table 5 2 Impedance values for various load materials and sizes

Utensil	Diameter (mm)	L (μH)	R (Ω)
C I -1	190	185	5 98
C I -2	170	194	5 48
C I -3	155	194	5
C I -4	120	201	3 86
S S 1-1	185	148	6 85
S S 1-2	165	160	5 48
S S 1-3	150	168	5 01
S S 1-4	130	174	4 31
S S 2-1	165	185	5 19
S S 2-2	150	186	4 7
S S 2-3	130	192	4 01
S S 2-4	110	195	3 56
S S 3-1	140	191	4 08
S S 3-2	230	168	7 25
S S 3-3	320	185	7 43
S-1	240	182	6 08
S-2	190	186	6 03
S-3	110	198	3 57

It is also interesting to observe the evolution of the load as a given utensil is displaced on the hob Such a measurement has been made for the greatest diameter in "sandwich" material A movement of 2 cm along the same radius was made between each measurement, the first measurement being made centred The result is shown compared

to the results for the other measurements of the same material in Fig 5.7. The relevant results are given in Table 5.2 It is clear that a movement of the utensil and a reduction in its diameter do not cause variations along the same line.

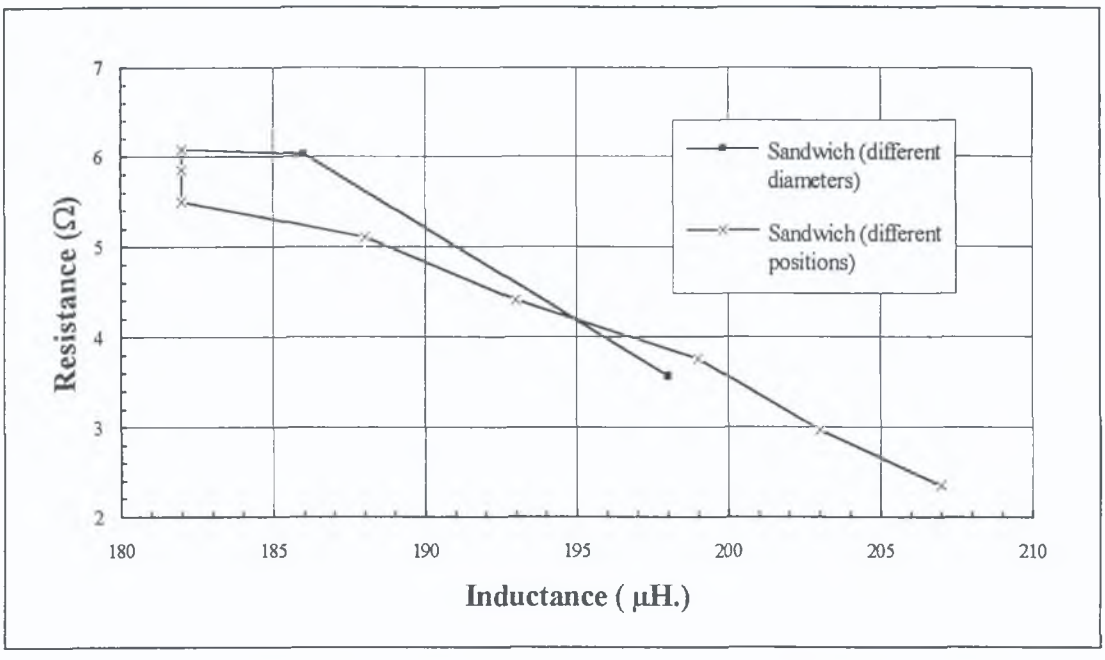

Figure 5.7: Comparison of impedance values given by variations in position and diameter for a given material.

Table 5.3: Impedance values for seven positions of the utensil S-1.

Utensil	Displacement from centre (mm.)	L (μH)	R (Ω)
S-1(p1)	20	182	5.85
S-1(p2)	40	182	5.5
S-1(p3)	60	188	5.11
S-1(p4)	80	193	4.41
S-1(p5)	100	199	3.76
S-1(p6)	120	203	2.97
S-1(p7)	140	207	2.35

5.5. Conclusions

The laws governing the equivalent impedance of an inductor are complex. For this reason, a valid measurement technique is essential. The results given by the measurement technique proposed are better than those given by the low-power RLC-bridge measurement. For the circuit designer, simulation allows the determination of the

worst case conditions for a more precise dimensioning of the switches and the switching-aid and resonating capacitors But this tool is useful wherever these impedances are studied, as a means of verification for load simulation software or in order to develop utensil alloys in a less empirical manner

This technique could also make possible the use of a micro-processor based on-line control architecture In this approach the load impedance would be identified using the Recursive Least Squares (RLS) algorithm and then used to calculate the α and ω of the resonant circuit The limit frequencies described in section 4 5 2 and the steady-state peak and switching current can be calculated from α and ω With this information it is possible to monitor the generators working (e g losses, proximity to critical working points) and limit the power or switch off as necessary

The RLS time increment will be a critical factor in the implementation of this control structure The off-line identification was carried out with a time interval of 100 ns This could probably be increased but not higher than 1 µs in order that (5 2) remain valid A current transformer will convert the load current to a voltage and three separate analog to digital converters will be necessary to ensure simultaneous measurements of the voltages in question These will need a conversion time that is less than the RLS time increment although it can be very near since the conversion time will be masked by the data processing A hardware synchronisation will provide the information that the converter is going through a switching transition in order to avoid processing data measured during this time After each switching transition, it will be necessary to re-initialise the increment counter In spite of the small dimensions of X, the RLS algorithm necessitates a certain number of multiplication operations Given the time factor, it will be necessary to carry these out either in a hardware manner or with the help of a dedicated co-processor

The implementation of this control structure will allow the suppression of the "Peak detector", "Low-pass filter" and "Current limitation circuit" shown in the control circuit in Fig 2 14 since the power level coming from the micro-processor will already have been adjusted to take into account the load conditions

General Conclusion

The technique for steady-state analysis of the induction SRC is a valid extension of the known state plane analysis methods. The simplicity of this technique gives a powerful tool to the circuit designer, who can readily calculate the steady-state parameters for a given load, supply and control condition. This will allow him to situate the zone in the L/R-plane within which the circuit can safely work without component stress. It can then be used to compare different control schemes (section 4.3.) and to tune the control algorithm.

However that is not the full extent of its impact. This technique draws attention back to the fact that it is not absolutely necessary to use the capacitor voltage, v_C, in order to work in the state plane. In fact the use of the inductor voltage, v_L, constitutes a very useful approach for two reasons:

(a) The voltage transitions are visible directly on the state plane trajectory and can be exploited as shown in section 4.5..
(b) A non-resonant circuit with only an inductive element can also be analysed (section 2.4.).

This opens up a whole range of switched mode power circuits using one or more switches that are inaccessible to the traditional state plane approach. For example this technique is being applied to an alternating current inverter for a metal halide lamp.

The didactic possibilities of the technique in general are undeniable for a circuit which has an additional degree of complexity with respect to the traditional power supply circuit. The circuit model can be introduced in its simplest form with its appropriate trajectory. The initial model can then be explored in terms of the variation in the trajectory for a modification of the model. The significance of each modification can be explained by comparing the relevant trajectories. In this manner, it is possible to come to a good understanding of the significance of each model component. As a subject for further research, this approach could be used in a computer program with a powerful graphical interface in order to allow variation of the circuit load, supply and control parameters in real time. This could serve design and academic purposes.

The load analysis technique presented is a useful tool for working in the induction environment in general. Its global approach should allow a wide range of applications. Further research could be carried out on the nature of the discrepancy between RLC-bridge measurements and those carried out using the least-squares analysis technique presented. This would help to pin-point the critical parameters of a material. Research on a new control architecture based on this load measurement technique as described in section 5.5. would have to define an optimum RLS algorithm time increment. This

parameter directly influences the technology that will be adopted for the A/D converters (i e successive approximation or flash) and the hardware necessary for the high-speed processing of the data (i e hardware multiplication before A/D conversion or software using a dedicated co-processor) There is no doubt that such a control algorithm will react sufficiently rapidly for the load variation which has a shortest time constant of the order of 20 ms due to mechanical inertia The difficulty resides in finding a sufficiently rapid measurement and calculation cycle to ensure the precision of the derived load parameters

References

[1] Dawson, F P , Jain, P , *Systems for induction heating and melting applications a comparison of load commutated inverter,* IEEE Power Electronics Specialists Conference, pp 281-290, 1990

[2] *Le chauffage par induction,* Departement applications de l'electricite, Direction des etudes et recherches, Electricite de France

[3] Kamli, M , Yamamoto, S , Abe, M , *A high-frequency half-bridge inverter for induction heating applications using insulated gate bipolar transistors (IGBT's),* EPE Proceedings, vol 1 pp 470-474, Firenze, 1991

[4] *Les applications innovantes de l'induction dans l'industrie,* Graphipress, Paris, 1992

[5] Ferrieux, JP , Keradec, JP , Baudon, Y , *A series-resonant inverter for induction heating,* E P E Proceedings, vol 1, Grenoble, 1987

[6] Rilly, G , Morizot, G , *Induction cooking appliance 2x5 kW,* E P E Proceedings, vol 1, Brussels, 1985

[7] Morizot, G , *Etude d'une table de cuisson a induction et convertisseur moyenne frequence, 2 kW, associe,* Conservatoire National des Arts et Metiers, Dijon, Memoire presente en vue d'obtenir le Diplôme d'Ingenieur C N A M , March 1981

[8] Hamill, D C , *Phase-locked induction heating inverter employing power mosfets,* Electronic Letters, March 1988, vol 24 no 7, pp 439-440

[9] Omori, H , Nakaoka, M , *New single-ended resonant inverter circuit and system for induction-heating cooking apparatus,* Int J Electronics, 1989, vol 67 no 2, pp 277-296

[10] Gaspard, JY , Maklouf, B , Burais N , *Cuisson par induction systeme inducteur evolue et modele mathematique associe,* Revue Generale de l'Electricite - N° 6 - June, 1992, pp 73-78

[11] Ferrieux, JP , Barbaroux, J , Ernst, R , *Generateur a induction pour la cuisson professionnelle,* Congres Europeen L'Induction et ses Applications Industrielles, Strasbourg, March 1991

[12] Hinchcliffe, S , Hobson, L , *Voltage-fed transistorised induction heating power supply,* Electronic Letters, May 1987, vol 23 no 11, pp 549-551

[13] Gaspard, JY , Maklouf, B , Burais, N , *Cuisson par induction une nouvelle generation de systemes inducteurs,* Congres europeen pour l'induction et ses applications industrielles, Strasbourg, March 1991

[14] Gaspard, JY , Maklouf, B , Burais, N , *Systemes inducteurs une nouvelle generation pour la cuisson professionnelle,* La Technique Moderne - N^{os} 5 - 6, 1991

[15] Witulski, A F , Erickson, R W , *Steady-state analysis of the series-resonant converter,* IEEE Transactions on Aerospace and Electronic Systems, vol 21, no 6, pp 791-799, 1985

[16] Vorperian, V , *Approximate small-signal analysis of the series and parallel resonant converter,* IEEE Transactions on Power Electronics vol 4, no 1, pp 15-24, 1989

[17] Sooksatra, S , Lee, C Q , *PWM controlled SRC with inductive output filter at constant switching frequency,* IEEE Power Electronics Specialists Conference, pp 258-265, 1990

[18] Klaasens, J B , *Analysis of a full-bridge series-resonant power interface with a bipolar power flow for a cyclic stable mode of operation,* E P E Proceedings, vol 1, Grenoble, 1987

[19] Cheron, Y , *La commutation douce dans la conversion statique de l'energie electrique,* Lavoisier, Paris, 1989

[20] Lee, C Q , Sin, K , *Analysis and Design of series Resonant Converter by State-plane Diagram,* IEEE transaction on Aerospace and Electronic Systems vol 22, no 6, pp 757-763, Nov 1986

[21] Ferrieux, JP , Forest, F , *Alimentations a decoupage convertisseurs a resonance principes modelisation composants,* Collection Technologies, Masson, Paris, 1987

[22] King, R , *A Fourier analysis for a fast simulation algorithm,* IEEE Transactions on Power Electronics, vol 4 no 4, October 1989

[23] Sadarnac, D , *Les alimentations a frequence de decoupage elevee,* Collection de la Direction des Etudes et Recherches d'Electricite de France, Editions Eyrolles, Paris, 1993

[24] Vorperian, V , Cuk, S , *A complete d c analysis of the series resonant converter,* IEEE Power Electronics Specialists Conference Record, M I T , Cambridge, Mass , June 1982, pp 85-100

[25] Foch, H , Escaut, B , Marty, P , Arches, M , Metz, M , *Hacheurs et onduleurs autonomes,* L E E I, 1985, section E 10 pp 1-4

[26] Rilly, G , *Contribution a l'utilisation des transistors de puissance en commutation, application a l'excitation du cathoscope "A 67 610 X PI",* U E R de Physique de l'Universite de Nantes, These pour le titre de Docteur-Ingenieur, 1976

[27] Ernst, R , Garnier, C , *Mesure numerique des caracteristiques d'un circuit oscillant pour le chauffage par induction,* Revue Generale de l'Electricite - N^{o} 8 - Sept , 1989

[28] Namjoshi, K V , Birringer, P P , *Electromagnetic coupling between heater coils of axial induction heaters*, IEEE Transactions on Magnetics, vol 26 no 5 September 1990

[29] Delage, D , Ernst, R , *Modelisation electrique d'un systeme de fusion par induction en creuset froid*, Revue Generale de l'Electricite - N° 4 - April, 1983, pp 266-272

[30] Fouladgar, J , Feliachi, J , Devely, G , *Distribution de l'energie dans un cylindre chauffe par induction*, Revue Generale de l'Electricite - N° 2 - February, 1991, pp 1-4

[31] Iskierka, S , *Numerical analysis of progressive heating through induction*, Revue Generale de l'Electricite - N° 2 - February, 1991, pp 5-11

[32] Delage, D , Ernst, R , *Prediction de la repartition du courant dans un inducteur a symétrie de revolution destine au chauffage par induction MF et HF*, Revue Generale de l'Electricite - N° 4 - April, 1984, pp 225-230

[33] Gaspard, JY , *Modelisation et realisation de nouveaux systemes de cuisson par induction*, These de Docteur, Ecole Centrale de Lyon, 1993

[34] Thomson Semiconductors, *The power transistor in its environment*, Graphic Express, Paris, 1984

[35] Clemente, S , Dubhashi, A , Pelly, B , *IGBT characteristics and applications*, International Rectifier Application Notes, AN-983, El Segundo, California

[36] Rilly, G , *DC-AC Converter for a load with an inductive component*, U S Patent ref 4,614,998, Sept , 1986

[37] Rilly, G , *Inverter for supplying a load having an inductive component*, U K Patent ref GB 2 175 154 A, Nov , 1986

[38] Kazimierczuk, M , Morse, W , *State plane analysis of zero-voltage-switching resonant dc/dc power converters*, IEEE National Aerospace and Electronics Conference Proceedings, Daytona, 1987, pp 433-440

[39] Franklin, G F , Powell, J D , Workman, M L , *Digital Control of Dynamic Systems*, Addison-Wesley, 1990

[40] Wellstead, P E , Zarrop, M B , *Self-Tuning Systems*, Wiley, 1991

[41] Foch, H , Marty, P , Roux, J , *Use of duality rules in the conception of transistorised converters*, PCI Proceedings, Munich 1980, 4B3, 1 to 11

[42] Cheron, Y , *Application des regles de la dualite a la conception de nouveaux convertisseurs a transistors de puissance Synthese du Thyristor-dual Domaine d'application*, These de Docteur-ingenieur, INP Toulouse, 1982

[43] Foch, H , Roux, J , Escaut, B , *Convertisseur moyenne frequence a transistor de puissance en 380v, application au chauffage par induction*, Electronique Industrielle No 50, April 1983

APPENDIX A: STEADY-STATE ANALYSIS BASED ON V_C

A.1. Limit cycle

This analysis is very similar to the one presented in the main text, except that the constructions are more complicated. This is the reason that the states v_L and v^* were preferred for the explanation of the principle and any exploitation of it. As can be seen from (3.6) and (3.7), the trajectories of V^{**} and V_C rotate clockwise unlike V^* and V_L for the case of free oscillations (see Fig. A.1).

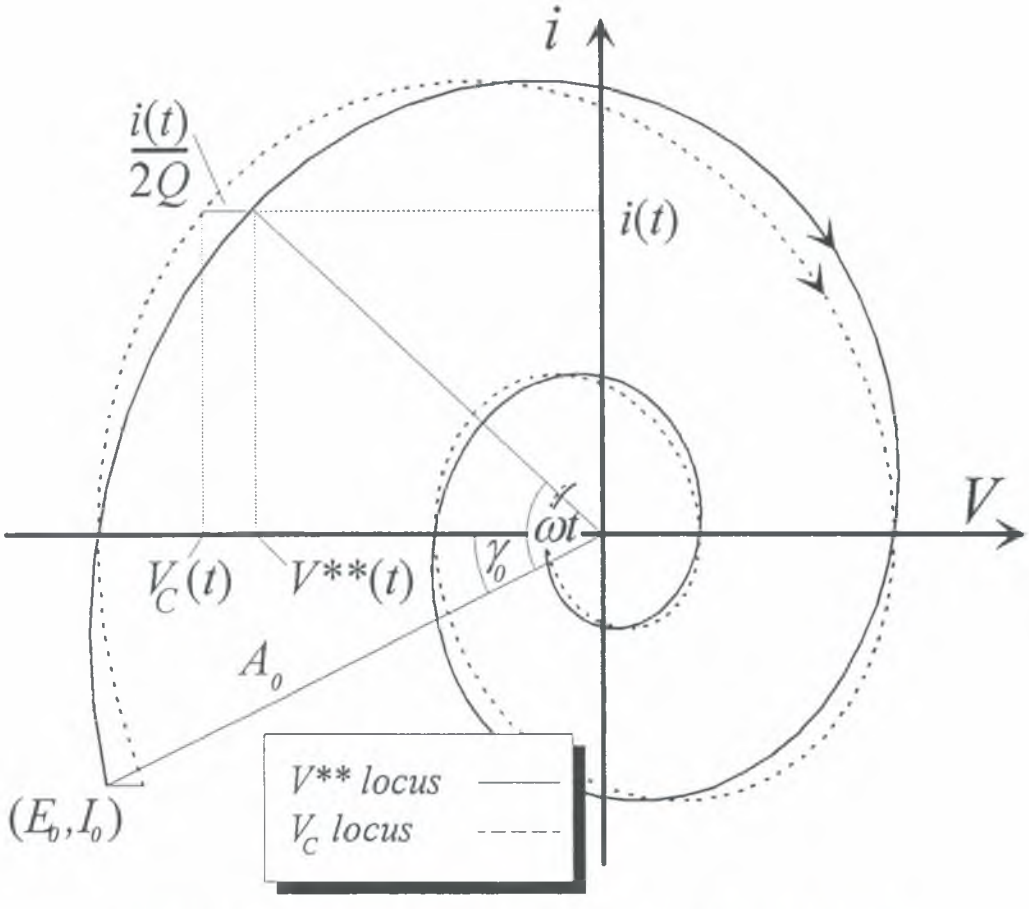

Figure A.1: Trajectory of V_C and V^{**} loci for free oscillations.

Using the loop equation for the two cases involved in forced oscillations, and the trajectory in Fig. 3.6, the steady-state trajectories of V_C and V^{**} can be derived. Their positive half-cycles are centred at the point $(\frac{V_s}{\omega L},0)$, while their negative half-cycles are centred at the point (0,0). The relevant trajectories are shown in Fig. A.2. The

switching points in the V_C and V^{**} trajectories are discontinuities in the slope in the same manner as with the power supply circuit (see section 1 3 2)

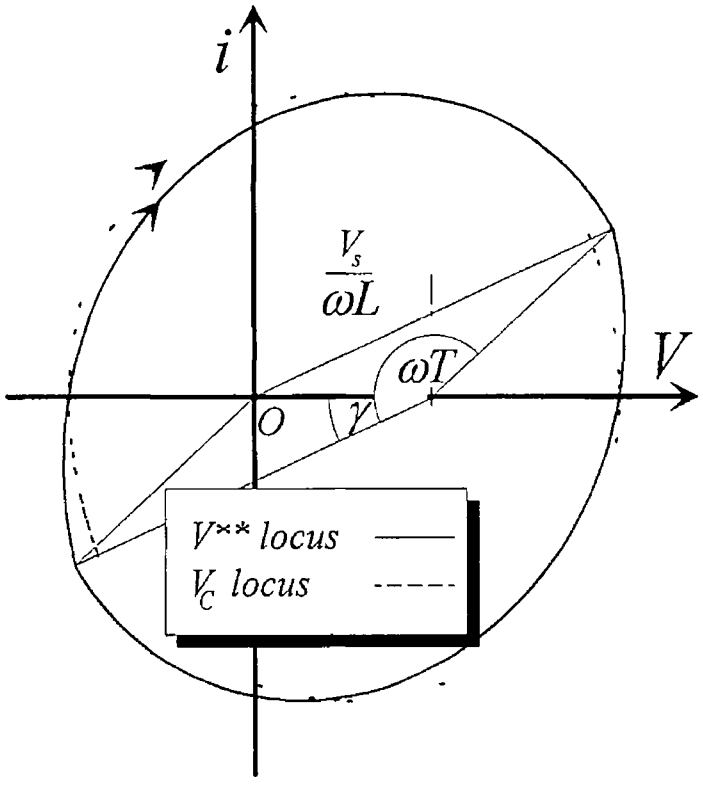

Figure A 2 Limit cycle of V_C and V^{**} loci

A 2 CCM 1 - *T* control

The construction can be done in the following manner (refer to Fig A 3)

- Draw a line PP' and bisect it to situate the point R
- Draw the spiral in question around the point R, in a counter-clockwise direction
- Situate the point U, at the intersection of the spiral and a line drawn through R at an angle, ωT, to PP'
- Draw the line PU, and bisect it at S
- Draw a line through S and R This is the voltage axis
- Now, $V_s = 2|SR|$, and the origin can be situated as shown

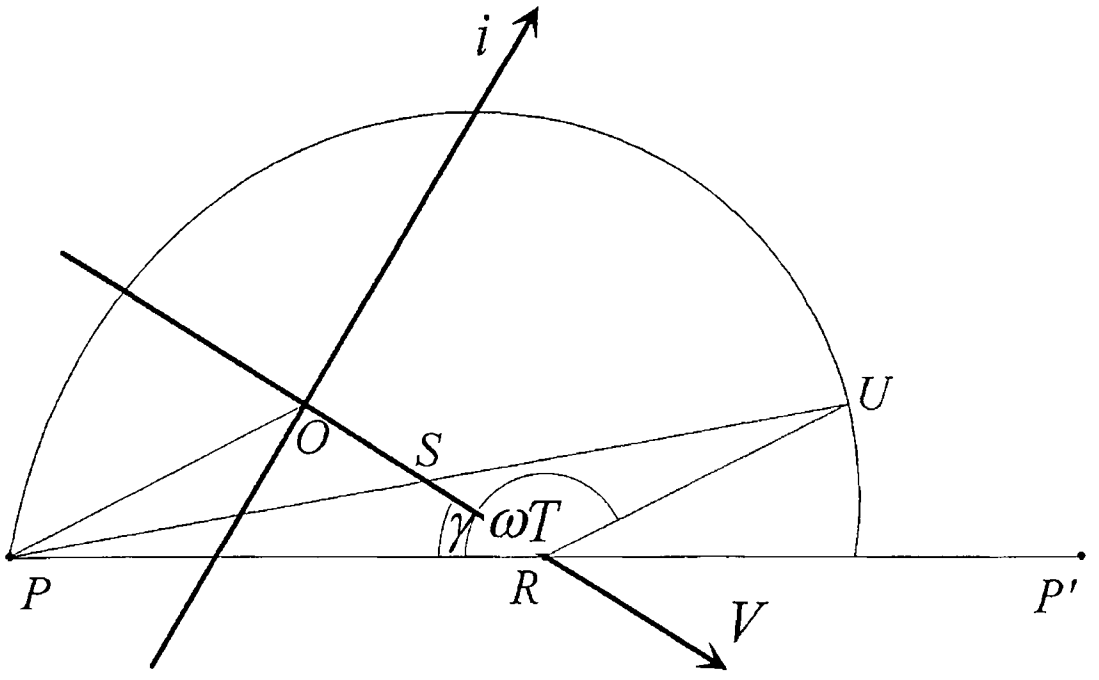

Figure A 3 Construction of V^{**} locus knowing periodic time, T

A 3 CCM 1 - T_C control

Once again this construction is similar to that presented for v_L and v^* It is based on the fact that a line drawn through the point U, parallel to the voltage axis, passes through P' (see Fig A 3) This is true because ΔPOR and $\Delta RUP'$ are identical triangles This conclusion can be drawn if the figure $POUR$ is a parallelogram and

$$|PR| = |RP'|$$

Now $POUR$ must be a parallelogram given that, by construction

$$|PS| = |SU|$$
$$|OS| = |SR|$$

The angle $\angle RUP' = \omega T_C$, and the construction is carried out as before

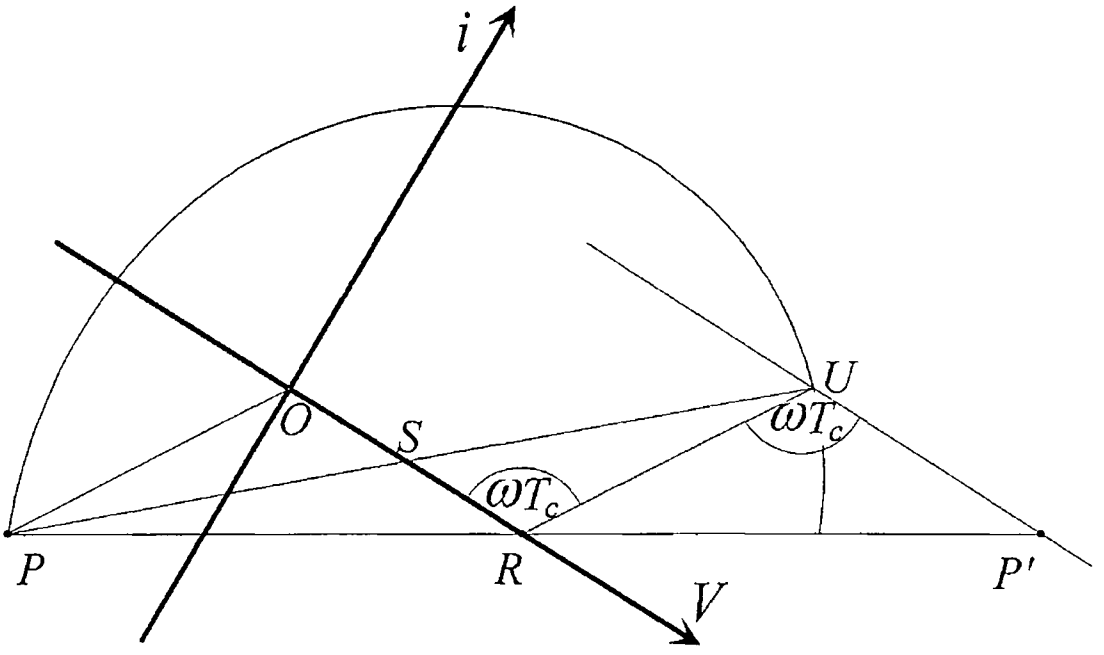

Figure A 4 V^{**} locus construction knowing transistor conduction time, T_c

APPENDIX B ANALYTIC APPROACH TO STEADY-STATE OPERATION WITH *T* CONTROL

The steady-state for a frequency, f, where

$$T = \frac{1}{2f} \tag{B 1}$$

can also be found analytically by appealing to the symmetry of the limit cycle
By symmetry $\gamma_0 = \gamma_1 = \gamma$

$$-A_0 \sin\gamma = -A_0 e^{-\alpha t} \sin(\omega T - \gamma)$$
$$\sin\gamma = e^{-\alpha t} \sin(\omega T - \gamma) \tag{B 2}$$

and

$$A_0 \cos\gamma - \frac{1}{2Q} I_0 = -A_0 e^{-\alpha T} \cos(\omega T - \gamma) + \frac{1}{2Q} I_1 + \frac{V_s}{\omega L} \tag{B 3}$$

(1) gives

$$\gamma = \tan^{-1}\left(\frac{\sin\omega T}{e^{\alpha T} + \cos\omega T}\right) \tag{B 4}$$

(2) and $I_1 = -I_0$ give

$$A_0 \cos\gamma = -A_0 e^{-\alpha T} \cos(\omega T - \gamma) + \frac{V_s}{\omega L} \tag{B 5}$$

$$A_0 = \frac{V_s}{\omega L\left(\cos\gamma + e^{-\alpha T} \cos(\omega T - \gamma)\right)} \tag{B 6}$$

However, these expressions give no physical insight into the operation of the converter in the manner that the state plane analysis does